Manipulation of Feshbach resonances in ultracold atomic collisions using time-dependent magnetic fields

F. H. Mies, E. Tiesinga, and P. S. Julienne
Atomic Physics Division, National Institute of Standards and Technology, 100 Bureau Drive Stop 8423, Gaithersburg, Maryland 20899-8423
(Received 17 August 1999; published 18 January 2000)

We have calculated the time-dependent dynamics of two ultracold Na atoms in an atom trap where a time-dependent magnetic field $B(t)$ moves a Feshbach resonance state across the energy threshold for a binary collision. Our coupled-channel scattering calculations, which reproduce the observed properties of such resonances in sodium atom collisions, can be reduced to an effective two-channel configuration-interaction model for one bound state and one continuum. The model is adapted to describe the time-dependent dynamics induced by $B(t)$ for two atoms trapped either in a strongly confining single well of an optical lattice or in an optical potential in the presence of a Bose-Einstein condensate. We show that a simple Landau-Zener curve crossing model gives quantitative agreement with exact calculations of field-induced transition rates. If $B(t)$ sweeps the resonance across threshold from above, two atoms in the ground state of the trap potential can be efficiently converted to translationally cold dimer molecules. If the resonance is swept from below, the atoms can be removed from the ground state and placed in hot vibrational levels of the trap. Our calculations reproduce the rapid atom loss rates observed in a Na Bose-Einstein condensate due to sweeping a Feshbach resonance state through the binary collision threshold.

PACS number(s): 34.20.−b, 34.10.+x, 34.50.−s

I. INTRODUCTION

Early in the study of the collision dynamics of ultracold atoms Tiesinga and co-workers [1,2] brought attention to the important role Feshbach resonances in atom-atom collisions might play both in determining loss mechanisms, and in the manipulation of the sign and magnitude of scattering lengths for the purpose of affecting the properties of a Bose-Einstein condensate (BEC). In particular it was suggested [1,3] that the Zeeman effect induced by a static magnetic field B might be used to move the resonance into a favorable position near the zero-energy collision threshold. The field could then be fine tuned to achieve a desired effect. Since that time several experimental results involving alkali atoms in ultracold traps above the critical Bose-Einstein condensation temperature [4–6], as well as in condensates [7,8] have been interpreted in terms of such resonance phenomena. Of course these observations have been complemented by many theoretical studies which have found such resonances manifest in the close-coupled scattering calculations for the alkali atoms (see review in Ref. [9]).

In this paper we will (1) develop exact scattering calculations to represent the threshold collision of two Na atoms in a magnetic field, (2) show how a two-channel configuration-interaction (CI) model is sufficient to represent the effect of the Feshbach resonance on the scattering, (3) adapt the continuum scattering model for the discrete energy levels of two atoms in a trapping potential, (4) calculate the transition probability out of the initial state of two atoms in the trap when a time-dependent magnetic field $B(t)$ sweeps a resonance through the threshold region, and (5) show that a simple Landau-Zener curve crossing model quantitatively explains our results. There are at least three different problem areas for which the model we develop is relevant. First, it explains the unexpectedly large loss of atoms from a Na BEC in a recent experiment at the Massachusetts Institute of Technology (MIT) which used a time-dependent B field to sweep a Feshbach resonance through the collision threshold region [7,8]. Second, it predicts that translationally cold diatomic molecules can be made efficiently in optical traps or lattices by using such $B(t)$ fields. Finally, since atomic collisions in optical lattices have recently been proposed for conditional quantum logical operations in quantum computing [10,11], our model should be useful for exploring the possible role of Feshbach resonances in such a context.

The sodium BEC experiments of Refs. [7,8] observed two distinct types of unexplained atom loss. In one experiment, $B(t)$ was slowly varied and then stopped in order to bring a resonance close to but not through the threshold region. An obvious mechanism for enhanced atom loss is a collision with a third atom that supplies or removes energy from the diatomic collision complex [12,13]. Reference [13] proposed a resonance-enhanced three-body mechanism with a three-body rate constant γ_d which is adjusted to fit the observations. This mechanism is likely to provide the dominant atom loss for this first type of MIT experiment. In a second MIT experiment, $B(t)$ was rapidly ramped to move the resonance state across the threshold region. The two-body mechanism we propose in this paper explains the enhanced atom loss in this case; a related picture derived from the coupled atom-molecule Gross-Pitaevskii equations for the system has been proposed by van Abeelen and Verhaar [14]. The two-body mechanism is a rigorous result associated with binary resonance scattering, and does not require the introduction of any adjustable parameters. Essentially, a nonconservative time-dependent magnetic or optical [15] field can also act as a

''third body'' and induce energy transfer and offer a loss mechanism. Significant population can be transferred to other energy states of the atom pair, depending on the ramping rate $\partial B/\partial t$ of $B(t)$. When the Feshbach resonance crosses the zero-energy threshold from below, the atom pair will gain energy from the magnetic field and be excited into higher-kinetic-energy states, effectively heating the trapped atoms. In contrast when the resonance crosses the zero-energy threshold from above we find that we can transfer significant, and under proper conditions, all, the population from the initial state via the resonance state into the highest lying vibrational level of the molecular dimer. By this mechanism we propose that an ensemble of ultracold alkali atoms can be efficiently converted into an ensemble of ultracold molecules. These molecules will be in a very high, but well prescribed vibrational level, and will be translationally and rotationally ultracold.

The remainder of the paper is divided into the following sections. Section II summarizes the *time-independent* multichannel close-coupled (CC) scattering calculations that underlie our modeling of two interacting atoms in a time-dependent magnetic field. For a static magnetic field interacting with a pair of ultracold atoms it is a simple matter to solve the time-independent close-coupled scattering equations and calculate the binary elastic and inelastic collision dynamics amongst the field-dressed atomic hyperfine states [16]. The main purpose of this section is to demonstrate that the exact CC calculations for two Na atoms in their lowest hyperfine state can be reduced to a time-independent CI model [17] involving a single isolated resonance state n and a single open channel or continuum state. In this case there is only elastic scattering. The CI model will allow us to extract a Fano-Beutler-type [18] expression for the resonance enhanced elastic scattering phase shift, i.e.,

$$\xi(\epsilon,B)=\xi_{bg}(\epsilon)-\tan^{-1}\frac{\Gamma_n(\epsilon)}{2[\epsilon-\epsilon_n^{res}(B)]}, \tag{1}$$

where $\xi_{bg}(\epsilon)$ is the elastic scattering phase shift in the absence of the resonance. By choosing B the Feshbach resonance with field dependent energy $\epsilon_n^{res}(B)$ can be brought into coincidence with the scattering state at kinetic energy ϵ. The strength of the resonance coupling is measured by a width $\Gamma_n(\epsilon)$, which obeys the Wigner threshold law [19] and varies as $\sqrt{\epsilon}$ at threshold. The MIT group [7,8] used the $\epsilon \to 0$ limit of Eq. (1) to interpret the experimentally observed Na scattering length as a function of B.

Section III introduces the modifications that are imposed on the time-independent CI model when the boundary conditions associated with a confining trap are imposed on the continuum state of the atom pair. The scattering continuum is transformed into a discrete set of states $|\epsilon_v\rangle$ for $v=0,1,\ldots$ with energy $\epsilon_v>0$. The ''true'' bound states of the dimer with $\epsilon_v<0$ will be labeled by $v=-1,-2,\ldots$. The matrix element $V_{n,v}$ which defines the coupling between the resonance state n and the discrete state $v\geqslant 0$ is obtained by making the substitution

$$2\pi V_{n,v}^2 \equiv \Gamma_n(\epsilon_v)\frac{\partial \epsilon_v}{\partial v}, \tag{2}$$

where $\partial v/\partial \epsilon_v$ is the density of discrete trap states [20].

Section III introduces two different trapping potentials. The first is a spherical harmonic potential of frequency ω_o. This is a good approximation when the two interacting atoms are held in a tightly confining well of an optical lattice or belong to a confined but dilute and uncondensed ultracold gas. In this case the center-of-mass motion of two identical interacting atoms of mass m is rigorously separable from the relative motion, and the dimer experiences a trapping potential $U_{trap}(R)=(\mu/2)\omega_o^2R^2$, where R is the interatomic separation and μ the reduced mass of the pair, which must be added to the untrapped dimer interaction potential $U_{bg}(R)$. The eigenvalues satisfy the energies of a three-dimensional harmonic oscillator [21], shifted due to U_{bg}.

The second type of dimer trapping potential we use is a spherical confining box. The box forms a good model for the interaction of two atoms in the presence of a finite-sized BEC. The two atoms populate the lowest-energy box state and the radius L of the box is chosen in such a way that this trapping energy ϵ_0 equals the mean kinetic energy of the atoms in a condensate. The Appendix evaluates the mean kinetic energy per atom of a finite-sized condensate using a first-order correction to the Thomas-Fermi model [22], and estimates that L is on the order of the Thomas-Fermi radius of the condensate [23].

In Sec. IV we introduce into the trapped state CI model a time-dependent magnetic field $B(t)$ which is linear in time. The entire effect of $B(t)$ is to make the eigenvalue of the resonance state $\epsilon_n^{res}(B)$ a function of time, i.e.,

$$\epsilon_n^{res}(t)=\epsilon_n^{res}(B_0)+(\partial\epsilon_n^{res}/\partial B)\frac{\partial B}{\partial t}t, \tag{3}$$

where B_0 is the magnetic field at $t=0$. It is important to understand that this relatively simple time-dependent CI model is rigorously and quantitatively related to the exact five-channel close-coupled description of the Feshbach resonances. The simplicity comes from the fact that the resonances are very sparse and isolated, together with the fortuitous property that the entire time dependence of the Hamiltonian only manifests itself on the resonance eigenvalue in Eq. (3). In future applications we intend to generalize the CI model to include inelastic couplings to other open channels. This should be equally rigorous, but in that case the time-dependence will no longer be so neatly confined to a single CI parameter.

Section IV will show that the time-dependent CI model can be visualized as a single resonance state n crossing a sparse manifold of true dimer bound states $v<0$, and a dense manifold of trapped dimer states $v\geqslant 0$. In view of the close analogy of this multiple curve crossing problem to a Landau-Zener (LZ) curve crossing model [24] we were pleased to find excellent agreement between our exact numerical solutions and LZ crossing probabilities [25,26]. We

find the probability of *remaining* in a state v once the resonance n is swept through is given by the LZ expressions

$$p_v^{LZ}=\exp(-w_{n,v}^{LZ}), \quad w_{n,v}^{LZ}=\frac{2\pi|V_{n,v}|^2}{\hbar\left|(\partial\epsilon_n^{res}/\partial B)\dfrac{\partial B}{\partial t}\right|}. \qquad (4)$$

The probability of removing population is $1-p_v^{LZ}$. We will show that in the Wigner threshold regime the most critical parameter in determining the removed population is the relative kinetic energy ϵ_v. The population removed by the passing resonance state is ultimately deposited into the adjacent manifold of bound dimer or excited trap states depending on the direction of the sweep.

In Sec. IV A we demonstrate the possibility of forming ultracold alkali dimers in a tight harmonic trap where the population initially resides in the lowest trapped state $v=0$. If the magnetic field is such that the Feshbach resonance lies above the dimer dissociation threshold and is initially unpopulated, and if the magnetic field is swept such that the resonance position moves below threshold, then we can transfer the initial population from $v=0$ into true bound states. Actually the population transferred from $v=0$ now resides in the first accessible bound state $v=-1$, and we form an ensemble of molecules which are translationally and rotationally ultracold, but vibrationally very hot. This same mechanism can also be used to form dimers in a BEC.

In Sec. IV B we consider the excitation of trapped state populations when the magnetic field is swept upward. This can lead to a significant heating of the trapped population, and is demonstrated both for the tight spherical harmonic trap and for the weakly confining spherical box trap which simulates a BEC. Since the loss of population from the lowest box state mainly depends on ϵ_0, the loss rate is insensitive to whether the BEC is represented as a spherical harmonic potential or as a spherical box as long as the confining potentials have the same value for ϵ_0. Section IV C gives practical Landau-Zener expressions for the Na resonances.

In Sec. V we explicitly apply the Feshbach CI model to the BEC experiment at MIT. Using the theoretical LZ probabilities without introducing adjustable parameters, we obtain loss rates that are consistent with the observations of Refs. [7,8], but with the caveat that we are assuming that heating of a condensate leads to trap loss. We also discuss the effects of three body collisions on the time-dependent magnetic-field experiments in a BEC. A macroscopic description in terms of coupled Gross-Pitaevskii equations was developed by Timmermans *et al.* [12] and applied to the MIT experiments by Yurovsky *et al.* [13]. We show how the effects of resonance-enhanced three-body recombination can easily be incorporated into our microscopic scattering model using a Breit-Wigner expression [27] to describe the process. Our results and conclusions are summarized in Sec. VI.

II. TWO-ATOM SCATTERING THEORY

A. Five-channel close coupling

This section sets up the exact multichannel close-coupled scattering calculation for two freely colliding ^{23}Na atoms.

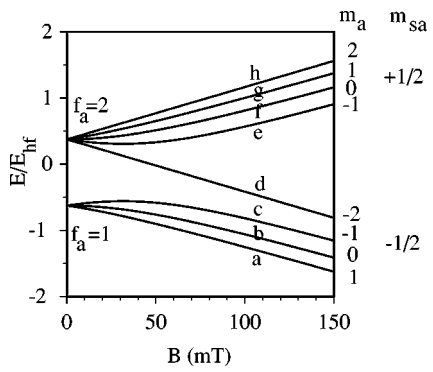

FIG. 1. The internal energy of a Na atom as a function of magnetic field. The states are labeled alphabetically. The quantum numbers are discussed in the text.

The formalism can be readily extended to other alkali species. The main purpose is to demonstrate that the CC calculation can be reduced to a configuration-interaction model [17] involving a single isolated resonance state and a single open channel or continuum state. The CI model will enable us to model a time-dependent magnetic-field sweep in subsequent sections.

For two interacting ^2S ^{23}Na atoms in an external magnetic field B, the relevant Hamiltonian for the dynamics of the relative motion contains a kinetic-energy operator, an atomic Hamiltonian for each of the atoms, and molecular adiabatic Born-Oppenheimer (ABO) potentials for the $X\,^1\Sigma_g^+$ and $a\,^3\Sigma_u^+$ states, where the molecular electron spin $\vec{S}=\vec{s}_a+\vec{s}_b$ is zero and 1, respectively. Weak spin-spin dipole interactions can safely be ignored for our purposes. The atomic Hamiltonian contains a hyperfine contact term that couples the electron spin to the nuclear spin and a Zeeman interaction [16] that couples the electron and nuclear spin to the magnetic field. The electron spin is denoted as $s_\alpha=1/2$, and the nuclear spin is denoted as $i_\alpha=3/2$ for atoms $\alpha=a$ or b, respectively.

The eight atomic eigenstates of each Na atom that diagonalize the hyperfine contact and Zeeman interaction are labeled $|a\rangle,|b\rangle,\ldots,|h\rangle$ in order of increasing (internal) energy, and are shown in Fig. 1. The projection m_α of $\vec{f}_\alpha=\vec{s}_\alpha+\vec{i}_\alpha$ along the magnetic-field direction is conserved. In the absence of a magnetic field f_α is conserved as well, such that the three atomic states $|a\rangle$, $|b\rangle$, and $|c\rangle$ are degenerate and correlate to $f_\alpha=1$, while the remaining states form the fivefold-degenerate $f_\alpha=2$ state. The $B=0$ energy splitting between the $f_\alpha=1$ and 2 states equals the hyperfine splitting E_{hf}. Note that throughout this paper we will express energy in temperature units by dividing any energy by the Boltzmann constant k_B. Thus, for Na, $E_{hf}/k_B=85.02$ mK. At large magnetic fields, where the Zeeman interaction dominates the hyperfine interaction, the bottom (top) four states have an electron spin $vecs_\alpha$ that is antiparallel (parallel) to the magnetic field. The projection of s_α along the magnetic field is $m_{s\alpha}$.

In the absence of the spin-spin interaction, the symmetry properties of the molecular Hamiltonian dictates that the magnetic quantum number $m=m_a+m_b$ and the mechanical

angular momentum l are conserved. For ultracold collisions it is sufficient to include only s-wave ($l=0$) scattering. Moreover, we consider scattering between two Na atoms, each in their lowest $|a\rangle$ hyperfine state (other cases could also be treated). Hence the magnetic quantum number m equals 2 and we see that there are only five combinations of atomic states that satisfy the $m=2$ and $l=0$ criteria. These are, in order of increasing internal energy, $|\{aa\}\rangle$, $|\{ag\}\rangle$, $|\{bh\}\rangle$, $|\{fh\}\rangle$, and $|\{gg\}\rangle$. The brackets indicate that the molecular states are symmetrized to account for the fact that Na atoms are composite bosons [16]. We introduce the simplified notation $|1\rangle$, $|2\rangle$, $|3\rangle$, $|4\rangle$, and $|5\rangle$ for these five states, which are also called scattering channels. In our calculations the zero of energy is always taken to be the separated atom energy of channel $|1\rangle$, irrespective of the magnitude of B. The colliding atoms are initially in the $|1\rangle$ channel. Given the very small collision energy $\epsilon \ll E_{hf}$, the other four channels are closed when the two atoms in channel $|1\rangle$ are infinitely far apart.

The asymptotic energies of channels $|2\rangle$–$|5\rangle$ depend on the magnitude of B. For $B=0$ channels $|2\rangle$ and $|3\rangle$ dissociate to E_{hf} and channels $|4\rangle$ and $|5\rangle$ dissociate to $2E_{hf}$. For $B\neq 0$ it is convenient to define δ_B such that the asymptotic energy separation between channels $|5\rangle$ and $|1\rangle$ equals $2E_{hf}+4\delta_B$. In this way $\delta_B \approx \mu_B B$ is approximately linear in B for field strengths at which the Feshbach resonances are observed. The magnetic moment $\mu_B/k_B=0.6717$ mK/mT equals the Bohr magneton.

We use a full close-coupled expansion of the total wave function [16] for a given B-field and a specific incident kinetic energy ϵ for the open channel $|1\rangle$, i.e.,

$$\Psi(\epsilon,B,R)=|1\rangle F_1(\epsilon,R)+\sum_{j=2}^{5}|j\rangle F_j(\epsilon,R) \qquad (5)$$

for $m=2$ s-wave scattering. The coupled equations introduce a 5×5 interaction matrix $\mathbf{W}(B,R)$ which is diagonal for $R\rightarrow\infty$ and dependent on the interatomic potentials of the $X\,^1\Sigma_g^+$ and $a\,^3\Sigma_u^+$ electronic states. The short-range off-diagonal matrix elements of $\mathbf{W}(B,R)$ are proportional to the ''exchange'' interaction, which is half the difference between the $a\,^3\Sigma_u^+$ and $X\,^1\Sigma_g^+$ potentials. The two ABO's have been carefully modeled by us to insure an excellent fit to the entire collection [28] of known spectroscopic Na_2 data and the observed Feshbach resonances [7,8] (see below). When the two electronic potentials have scattering lengths of $A_{S=0}=20.3a_o$ and $A_{S=1}=63.9a_o$ ($1a_o=0.0529177$ nm) respectively, a fit to all the data can be achieved for $B=0$. Our model gives $A_{f=1,m=-1}=54.6a_o$ for the Bose-Einstein-condensed $|c\rangle$ state, which agrees with other determinations within their stated uncertainties [29–31]. The value of $A_{S=1}$ is revised from our earlier determination [29], which reported $A_{S=1}=85\pm 3\ a_o$, and $A_{f=1,m=-1}=52\pm 5\ a_o$. The $X\,^1\Sigma_g^+$ and $a\,^3\Sigma_u^+$ states support 66 and 16 vibrational states, respectively.

The diagonal elements of the interaction matrix $W_{j,j}(B,R)$ define what we call the ''diabatic'' interaction potentials. At large R these are equivalent to the ''adiabatic'' potential curves $U_j(B,R)$ shown in Fig. 2, which are obtained by diagonalizing $\mathbf{W}(B,R)$ at each R. The figure shows three of the five diabatic potential curves for magnetic field strengths of 0 and 91 mT, respectively. The value of $B=91$ mT is slightly larger than the magnetic field values where Feshbach resonances in the $|\{aa\}\rangle$ collision are observed [7,8]. At any finite R, the five states are mixed by the off-diagonal exchange couplings in $\mathbf{W}$. For the internuclear separations shown in Fig. 2 the $X\,^1\Sigma_g^+$ and $a\,^3\Sigma_u^+$ ABO potentials are degenerate, the exchange couplings are negligible, and consequently all the curves are parallel with $U_j=W_{j,j}$.

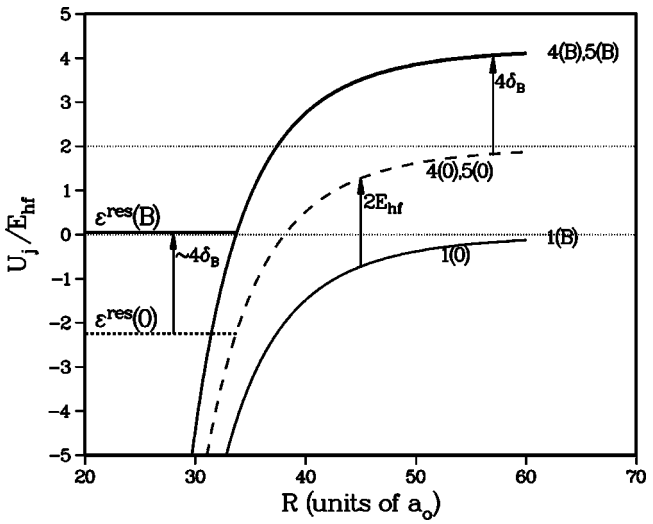

FIG. 2. Three of the five adiabatic potentials U_j of the $m=2$ s-wave scattering process are shown as functions of internuclear separation. The dashed curves correspond to $B=0$ adiabatic potentials and are labeled $j(0)$, while the solid curves correspond to $B=91$ mT adiabatic potentials and are labeled $j(B)$, where in general j is 1, 2, 3, 4, or 5 in order of increasing energy. However, for clarity the $j=2$ and 3 curves are omitted. For both B values the zero of energy is set at the $R\rightarrow\infty$ asymptote of the $j=1$ adiabatic potential. For the range of internuclear separation shown the adiabatic potentials 1(0) and 1(B) are identical. As is explained in the text, the two Feshbach resonances are due to weak coupling to bound states in the $j=4$ and 5 adiabatic potentials. The vibrational levels $\epsilon_n^{res}(0)$ and $\epsilon_n^{res}(B)$ show the relevant bound state for $B=0$ and $B=91$ mT, respectively. On the energy scale of the figure the $j=4$ and 5 Feshbach resonances are indistinguishable. The arrow labeled $2E_{hf}$ indicates the $B=0$ splitting between level 1(0) and levels 4(0) or 5(0). The arrows labeled $4\delta_B$ show that the energy shift of the asymptotic energies of state 5 from $B=0$ to $B=91$ mT is approximately equal to the energy shift of the bound states.

As we shall see from our close-coupled calculations, the pair of resonances seen in Refs. [7,8] originate from states $|4\rangle$ and $|5\rangle$, since we find that the position of the resonances relative to the open channel $|1\rangle$ threshold as a function of B varies almost perfectly as $4\delta_B$. At zero field both resonances begin as ''true'' five-channel bound states that exist well below the zero-kinetic-energy threshold for channel $|1\rangle$. In Fig. 2 this is indicated by the vibrational level marked $|\epsilon_n^{res}(0)\rangle$. The position of these resonances are well approximated by the vibrational eigenvalues defined by the adiabatic

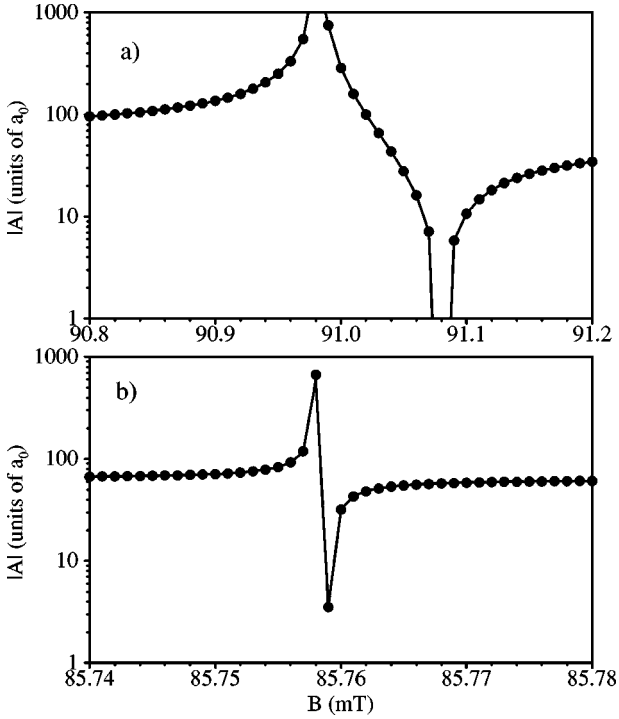

FIG. 3. The absolute value of the scattering length A vs the magnetic-field strength B evaluated in the vicinity of the strong [panel (a)] and weak [panel (b)] Na resonance. The filled dots are extracted from a close-coupling calculation for an incident kinetic energy ϵ of 1 nK. The curve passing through the dots fit the resonant expression $A_n = 62.8a_0\,[1-0.0975/(B(\mathrm{mT})-90.983)]$ for the strong resonance and $A_n = 63.8a_0\,[1-0.00095/(B(\mathrm{mT})-85.758)]$ for the weak resonance.

potentials $U_4(0,R)$ and $U_5(0,R)$, respectively. As the field strength is increased these levels becomes displaced and move to the position indicated by $|\epsilon_n^{res}(B)\rangle$. In the process of passing through the threshold the resonance states become degenerate with the continuum states associated with the open channel $|1\rangle$.

When the five coupled equations are solved numerically, an asymptotic analysis of the wave function gives the T matrix, which describes the transition amplitudes between all asymptotically *open* channels. The energy and magnetic-field dependence of the T-matrix allow us to define phase shifts and scattering lengths and to extract resonance widths and positions. Since in this case the $|1\rangle$ state is the only open channel, the asymptotic analysis of the energy-normalized wave function F_1 leads to

$$F_1(\epsilon,R) \rightarrow \sqrt{\frac{2\mu}{\pi\hbar^2}}\,\frac{\sin(kr+\xi(\epsilon))}{\sqrt{k}} \quad \text{for } R\rightarrow\infty, \qquad (6)$$

where $\epsilon=\hbar^2k^2/2\mu$, and μ is the reduced mass of the dimer. $\xi(\epsilon)$ is the phase shift and $T_{1,1}=1-\exp(2i\xi)$ describes the full T matrix. A scattering length is defined by $A=-\tan\xi/k$ in the limit $\epsilon\rightarrow 0$.

Figure 3 shows the magnetic-field dependence of the scattering length A, a property of $\epsilon\rightarrow 0$ scattering, near the two Feshbach resonances that are present in the ultracold $|\{aa\}\rangle$ collision. The scattering phase is actually evaluated at a kinetic energy $\epsilon=1$ nK, but this is well within the Wigner threshold region, so that A is independent of the actual choice of energy. These data fit very well to the resonance-like expression suggested by Eq. (1):

$$A(B) = A_{bg}\left[1-\frac{\Delta_n}{B-B_n^{res}}\right]. \qquad (7)$$

This expression, which will be justified later in this section, is identical to that derived in Ref. [3] and used in the analysis of Refs. [7,8]. Our theoretical results conform with this functional form and yield resonance positions $B_{n=s}^{res}=91.0$ mT [32] for the ''strong'' resonance and $B_{n=w}^{res}=85.8$ mT for the ''weak'' resonance, in excellent agreement with the experimentally observed values $B_s^{res}=90.7\pm 2$ mT [32] and $B_w^{res}=85.3\pm 2$ mT [7,8]. The calculated ''strong'' resonance width $\Delta_s=0.098$ mT is also confirmed by experiment. The ''weak'' resonance width $\Delta_w=0.00095$ mT is a factor of four larger than found by experiment. Our calculated resonance positions and widths are consistent with the calculations of van Abeelen and Verhaar [30] (also see Ref. [8]).

Figure 4 shows the $|T_{1,1}|^2 \equiv 4\sin^2\xi$ matrix element for elastic scattering in state $|1\rangle=|\{aa\}\rangle$ as a function of colli-

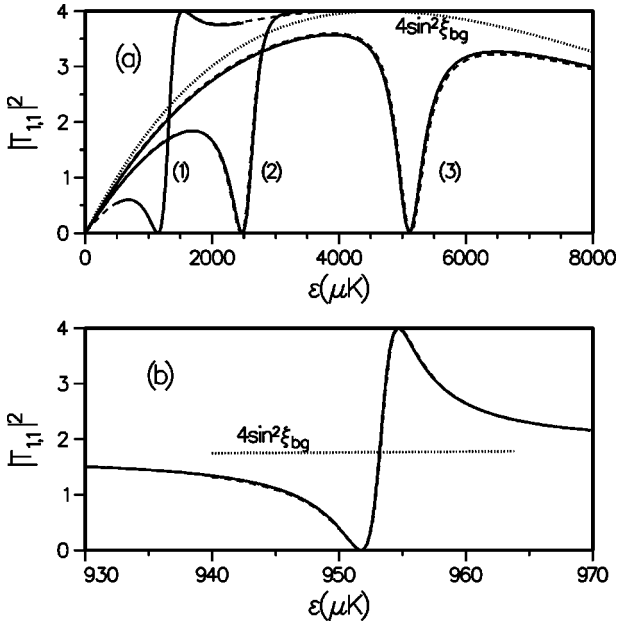

FIG. 4. The energy dependence of the square of the T matrix $|T_{1,1}(\epsilon,B)|^2$ for several magnetic-field strengths close to the field locations of the two Na Feshbach resonances. Solid lines correspond to numerical close-coupling calculations, dashed lines correspond to the results from a two-channel CI model, and dotted lines describes the background scattering in the absence of a resonance. Panel (a) shows results for (1) $B=91.5$ mT, (2) 92.0 mT, and (3) 93.0 mT close to the ''strong'' resonance. Panel (b) shows results for $B=86.15$ mT close to the ''weak'' resonance. Fits to Eq. (1), with $\Gamma_n(\epsilon)$ obtained from Eq. (24), gives for the four B field strengths $\epsilon^{res}/k_B=1300$ μK, 2550 μK, 5110 μK, and 4.00 μK, and $\Gamma_n(\epsilon^{res})/k_B=350$ μK, 440 μK, 520 μK, and 2.95 μK, respectively.

sion energy. The figure compares $|T_{1,1}|^2$ for magnetic-field strengths that are slightly larger than the calculated resonance positions, so that the resonance at $\epsilon_n^{res}(B)$ lies above the $\epsilon=0$ threshold. We find in all cases that $\epsilon_n^{res}(B)$ increases for increasing magnetic-field strength. In fact, the position of the resonances which are extracted by fitting to Eq. (1) are observed to vary as

$$k_B^{-1}\partial\epsilon_n^{res}(B)/\partial B = +2540\ \mu\text{K/mT}. \tag{8}$$

This closely follows the magnetic-field dependence of the splitting between hyperfine states $|1\rangle$ and $|4\rangle$ or $|5\rangle$.

B. Two-channel configuration interaction

The observed sparseness of resonances, and the excellent fit to the Fano-Beutler line shape of Eq. (1), suggest that the exact close-coupled wave function of Eq. (5) can be expressed in an *equivalent* CI form [17],

$$\Psi_n(\epsilon,B,R)\equiv|1,\text{CI}\rangle F_1(\epsilon,R)+A_n(\epsilon,B)|\epsilon_n^{res}(B)\rangle. \tag{9}$$

This CI expansion consists of a single open-channel continuum wave function $F_1(\epsilon,R)$ interacting with a single isolated resonance state $|\epsilon_n^{res}(B)\rangle$ which embodies the exact close-coupled interactions between the four closed channels. The resonance amplitude $A_n(\epsilon,B)$ is independent of R. The isolated R-dependent resonance state can be represented as a simple product state

$$|\epsilon_n^{res}(B)\rangle\approx|n(B)\rangle\phi_n^{res}(R), \tag{10}$$

where $|n\rangle$ consists of a *fixed* ϵ-independent combination of channel states [35]:

$$|n(B)\rangle\approx\sum_{j=2}^{5}|j\rangle a_j^n(B). \tag{11}$$

The CI wave function can be calculated using the two-channel Hamiltonian

$$H_n(B)=|1,\text{CI}\rangle\langle 1,\text{CI}|\{T+U_{bg}(R)\}+|n\rangle\langle n|\{T+U_n(B,R)\} +\{|1,\text{CI}\rangle\langle n|+|n\rangle\langle 1,\text{CI}|\}W_{n,1}(R), \tag{12}$$

where T is the radial kinetic-energy operator. We will construct effective potentials for the background continuum, $U_{bg}(R)$, for the resonance level $U_n(B,R)$, and for the coupling between them, $W_{n,1}(R)$. Our construction will be both simple and capable of reproducing the results of the full five-channel CC calculation. In this regard, it is useful, though not necessary, to introduce ideas from the multichannel-quantum-defect theory (MQDT) [33,34].

1. Open-channel effective potential

It is convenient to introduce a *single* reference potential $U_{\text{bg}}(R)$ for CI channel $|1,\text{CI}\rangle$, where this potential has the same long-range form and asymptotic energy as that for channel $|1\rangle$. When the reference potential is chosen to reproduce the exact background phase shift ξ_{bg} away from any resonance, $\xi=\xi_{bg}+\xi^{res}$ can be expressed as a sum of a background and resonance phase shift as in Eq. (1). This behavior is derived by noting that the exact open channel radial wave function F_1 in Eq. (9) can be asymptotically represented in MQDT form as a linear combination of the regular $s(\epsilon)$ and irregular $c(\epsilon)$ reference functions that are independent solutions of the Hamiltonian $T+U_{bg}(R)$ at collision energy ϵ:

$$F_1(\epsilon,R)\rightarrow\sqrt{\frac{2\mu}{\pi\hbar^2}}\cos\xi_n^{res}[s(\epsilon,R)-\tan\xi_n^{res}c(\epsilon,R)]. \tag{13}$$

This insures that away from resonance $F_1(\epsilon,R)=\phi_\epsilon(R)$, where $\phi_\epsilon(R)$ is the regular solution of

$$\left[-\frac{\hbar^2}{2\mu}\frac{d^2}{dR^2}+U_{\text{bg}}(R)\right]\phi_\epsilon(R)=\epsilon\phi_\epsilon(R) \tag{14}$$

and

$$\phi_\epsilon(R)\equiv\sqrt{\frac{2\mu}{\pi\hbar^2}}s(\epsilon,R)\rightarrow\sqrt{\frac{2\mu}{\pi\hbar^2}}\frac{\sin(kR+\xi_{bg})}{\sqrt{k}}. \tag{15}$$

The factor $\tan\xi_n^{res}$ which multiplies the irregular reference function, $c\rightarrow k^{-1/2}\cos(kR+\xi_{bg})$, embodies the effect due to the Feshbach resonance. The phase shift ξ_{bg} for elastic scattering by $U_{bg}(R)$, describes the physics in the absence of a resonance. The resonance contribution to the phase is [17,33,34]

$$\tan\xi_n^{res}(\epsilon,B)=\frac{\Gamma_n(\epsilon)}{2[\epsilon-\epsilon_n^{res}(B)]}, \tag{16}$$

where $\Gamma_n(\epsilon)$ is the resonance width. Equation (1) immediately follows.

We find that we obtain an excellent description of the exact close-coupled background phase shift ξ_{bg} by taking $U_{\text{bg}}(R)$ to be the diabatic potential $W_{1,1}(R)$. Furthermore, since the scattering length of the $W_{1,1}(R)$ potential is almost identical to the $63.9a_o$ scattering length of the $a\,^3\Sigma_u^+$ potential, we can simply equate $U_{\text{bg}}(R)$ to the $a\,^3\Sigma_u^+$ potential. The explanation for this simple behavior is as follows. At the magnetic-field strengths where the Feshbach resonances are observed, the electron spin of an atom in state $|a\rangle$ is nearly antiparallel to the magnetic-field direction, and the state $|1\rangle=|\{aa\}\rangle$ is predominantly of triplet character. Consequently the corresponding *diabatic* potential $W_{1,1}(R)$ is predominantly an $a\,^3\Sigma_u^+$ potential. At $R\approx 19a_o$ this diabatic potential crosses a predominantly $X\,^1\Sigma_g^+$ potential originating from channel $|2\rangle$ which is much deeper than the $a\,^3\Sigma_u^+$ potential for $R<19a_o$. However, the coupling is very weak, and hence the crossing is *diabatic* and can be neglected.

We actually use an even simpler analytic form for $U_{\text{bg}}(R)$ in our CI model,

$$U_{bg}(B_o,R)=\alpha\exp(\gamma(R_e-R))-\frac{C_6}{R^6}, \tag{17}$$

with $\alpha=8.24322\times10^{-3}$, $C_6=1562.155$, $\gamma=1.666$, and $R_e=13.02$, all in atomic units (length in a_o, energy in $e^2/a_o=4.359743\times10^{-18}$ J). Although this potential only supports five bound states, rather than the 16 that actually exist in the $a\,^3\Sigma_u^+$ potential, the parameters have been adjusted to insure that its long-range behavior, and especially the scattering length $a=63.9a_o$ and the position of the last bound state agree with the values for the exact potential. This is useful in Sec. III B below, since reducing the number of nodes in the short-range portion of the wave function reduces the numerical effort in evaluating CI matrix elements.

2. Closed-channel effective potential

The unit-normalized resonance vibrational state $\phi_n^{res}(R)$ at energy $\epsilon_n^{res}(B)$ satisfies the Schrödinger equation

$$\left[-\frac{\hbar^2}{2\mu}\frac{d^2}{dR^2}+U_n(B,R)\right]\phi_n^{res}(R)=\epsilon_n^{res}(B)\phi_n^{res}(R). \tag{18}$$

Given the linear dependence of the resonance position on B, as noted in the discussion of Fig. 4, we can infer that $U_n(R,B)$ depends linearly on B:

$$U_n(B,R)=U_n(B_o,R)+\frac{\partial\epsilon_n^{res}(B)}{\partial B}(B-B_o), \tag{19}$$

where B_o is a magnetic-field strength not too far removed from B_n^{res}.

The dependence of the resonance position on B allows us to be more specific about the shape of $U_n(R,B)$. The dependence conforms almost perfectly with the displacement of the $|4\rangle=|\{fh\}\rangle$ and $|5\rangle=|\{gg\}\rangle$ thresholds relative to the $|1\rangle=|\{aa\}\rangle$ threshold. Furthermore the adiabatic potentials that correlate to the asymptotic $|4\rangle$ and $|5\rangle$ channels correlate to the $a\,^3\Sigma_u^+$ potential at short distances. In fact the vibrational level positions of these two adiabatic potentials are in very good agreement with the vibrational level of the pure $a\,^3\Sigma_u^+$ potential. These observations demonstrate that the resonance in Eq. (11) is predominantly generated by channels 4 and/or 5 [35], and that the *resonance vibrational wave function* $\phi_n^{res}(R)$ is well approximated by the vibrational wave functions supported by a pure $a\,^3\Sigma_u^+$ potential. However, a CC calculation is necessary to obtain the exact *position* of the resonance, which depends on nonadiabatic mixing among the five channels in the problem.

To model the variation of $\epsilon_n^{res}(B)$ with B, it is both numerically convenient, and physically reasonable to take the resonance potential to be a shifted version of U_{bg}:

$$U_n(B_o,R)=U_{bg}(R)+\delta U_n(B_o). \tag{20}$$

Numerical tests confirm that ϕ_n^{res} is well approximated by the fourth bound state supported by U_{bg} in Eq. (17). This corresponds to the second level below threshold ($n=-2$) and mimics the properties of the exact (15th) resonance vibrational state associated with both of the observed MIT resonances. We merely must set the constant $\delta U_n(B_o)$ to insure that, for a chosen field strength B_o, the calculated eigenvalue $\epsilon_n^{res}(B_o)$ coincides with the corresponding CC resonance in Fig. 4. Once this is set the B-field dependence introduced in Eq. (19) will automatically shift the eigenvalue $\epsilon_n^{res}(B)$ as required. In Sec. IV we will make $B(t)$ a function of time and introduce the ramping of the magnetic field to simulate the MIT experiments.

3. CI width and threshold properties

The CI expression for the width $\Gamma_n(\epsilon)$ in Eqs. (1) and (16) is

$$\Gamma_n(\epsilon)\equiv2\pi|V_n(\epsilon)|^2=2\pi|\langle\phi_n^{res}|W_{n,1}|\phi_\epsilon\rangle|^2. \tag{21}$$

In the CC calculations, the width depends in a complex way on the off-diagonal matrix elements of the interaction matrix **W**, but the resonant position and width can easily be extracted by fitting the calculated resonance shapes, such as those in Fig. (4). Since the coupling of the resonance to the continuum depends on short-range interactions, we use the following *arbitrary* exponential form to simulate these couplings in the CI model:

$$W_{n,1}(R)=\beta_n e^{-0.2R}. \tag{22}$$

We choose β_n so that the width calculated from Eq. (21), agrees with the exact CC width. This fitting is done for the same field strength B_o that is used to chose $\delta U_n(B_o)$ in Eq. (20). In order to avoid the subtle energy dependences that are introduced by the threshold, we place the resonance we are fitting well above threshold. Once $\delta U_n(B_o)$ and β_n are set, the threshold effects will be properly and, for all intentions, exactly handled by the CI model. For the strong resonance in Fig. 4(a), we fit $\beta_n/k_B=2.156\times10^6$ μK using the $\epsilon_n^{res}/k_B=1300$ μK resonance with $\Gamma_n/k_B=350$ μK for $B_o=91.5$ mT. For the weak resonance in Fig. 4(b) $\beta_n/k_B=2.103\times10^5$ μK was found for the $\epsilon_n^{res}/k_B=953.4$ μK resonance with $\Gamma_n/k_B=2.95$ μK for $B_o=86.15$ mT. The agreement between the dashed and solid lines in Fig. (4) demonstrates the excellent quality of the CI model in describing the exact CC scattering.

For ultracold collision applications it is crucial to take into account the energy dependence of the width [20]. This Wigner threshold behavior can be derived from the energy dependence of the $C_1^{-2}(\epsilon)$ coefficient defined in the MQDT theory [33,20]. The unperturbed *energy*-normalized continuum wave function $\phi_\epsilon(R)$ associated with channel $|1\rangle$ in Eq. (15) introduces the Wigner threshold behavior through its dependence on the threshold parameter $C_1^{-1}(\epsilon)\to\sqrt{k}$, i.e., $s(\epsilon,R)=C_1^{-1}(\epsilon)f_1(R)$. The analytic function $f_1(R)$ is a solution of the Schrödinger equation for the reference potential and is uniquely defined by an ϵ-insensitive boundary condition at a small internuclear separation where the exchange splitting is large compared to the Zeeman and hyperfine interactions. Then it follows that

$$\Gamma_n(\epsilon)=\frac{4\mu}{\hbar^2}|\langle\phi_n^{res}|W_{n,1}|f_1\rangle|^2C_1^{-2}(\epsilon), \tag{23}$$

which can be rewritten as

$$\Gamma_n(\epsilon)=\Gamma_n(\epsilon_n^{res})\frac{C_1^{-2}(\epsilon)}{C_1^{-2}(\epsilon_n^{res})}\rightarrow\Gamma_n(\epsilon_n^{res})\sqrt{\frac{\epsilon}{\epsilon_n^{res}}}. \tag{24}$$

Equation (24) clearly shows the expected $\sqrt{\epsilon}$ dependence as $\epsilon\rightarrow 0$. The resonance state amplitude $A_n(\epsilon,B)$ in Eq. (9) is proportional to $V_n(\epsilon)$ [17],

$$A_n(\epsilon,B)\approx\frac{V_n(\epsilon)}{\sqrt{(\epsilon-\epsilon_n^{res})^2+\Gamma_n(\epsilon)^2/4}}, \tag{25}$$

and also exhibits appropriate Wigner threshold behavior.

The Wigner threshold behavior of $\Gamma_n(\epsilon)$ and $A_n(\epsilon,B)$ rests on the assumption that, except for its resonance position $\epsilon_n^{res}(B)$, the resonance wave function $|\epsilon_n^{res}(B)\rangle$ is not modified appreciably by B or ϵ. The resonance state wave function can then be factored as in Eq. (10). In our case this is justified since the matrix elements $W_{n,1}$ are short ranged. Except for a well-understood scaling $C^{-1}(\epsilon)$ associated with the asymptotic normalization of the open channel, both the reference wave function $\phi_\epsilon(R)$ and the resonance wave function $\phi_n^{res}(R)$ are otherwise insensitive to the asymptotic energy or to the magnetic-field strength.

Equation (7) for the scattering length near an isolated Feshbach resonance follows immediately from our CI analysis upon using Eq. (1) and the definition of scattering length, $A(B)=-k^{-1}\tan\xi(\epsilon,B)$, for $\epsilon\rightarrow 0$. Define the resonant field strength B_n^{res} as

$$\epsilon-\epsilon_n^{res}(B)=-\frac{\partial\epsilon_n^{res}(B)}{\partial B}(B-B_n^{res}), \tag{26}$$

and Δ_n as

$$\Delta_n=\frac{\partial B}{\partial\epsilon_n^{res}}\frac{\Gamma_n}{2kA_{bg}}, \tag{27}$$

where $A_{bg}=-k^{-1}\tan\xi_{bg}(\epsilon)$ for $\epsilon\rightarrow 0$ is the scattering length in the absence of the resonance. As $\epsilon\rightarrow 0$, Eq. (24) implies that Δ_n approaches a constant, and we recover Eq. (7) in Section II A. This equation is used in the analysis of Refs. [7,8]. We have already demonstrated in Fig. 3 the excellent agreement between our exact CC results for $A(B)$ at $\epsilon=1$ nK and the CI expression in Eq. (7).

III. TRAPPED STATES

A. Trapping potentials and vibrational levels

We now turn our attention to describing collisions in the presence of an external trapping potential which confines the atoms. We might envision the atoms to be confined in a single cell of an optical lattice [10,11] or in an optical trap such as used for the MIT BEC experiment [7,8]. When atoms are confined in a trap, we must add a trapping potential and replace U_{bg} by $\bar{U}_{bg}=U_{bg}(R)+U_{trap}(R)$. Although U_{bg} has a continuous spectrum with $\epsilon>0$ and corresponding energy-normalized continuum wave functions $\phi_\epsilon(R)$, $\bar{U}_{bg}$ has a discrete spectrum of vibrational eigenvalues ϵ_v with corresponding unit-normalized bound-state eigenfunctions ϕ_v,

$$[T(R)+\bar{U}_{bg}(R)]\phi_v(R)=\epsilon_v\phi_v(R). \tag{28}$$

We refer to the infinite set of levels with positive energy as ''trapped states'' or, sometimes, ''box-normalized continuum states.'' We chose the vibrational quantum numbers such that $v=0$ defines the lowest trapped state. We are especially interested in this first positive energy state ϕ_0, since we will generally assume that the entire trapped-atom population initially resides in this state. As we shall see, because of the Wigner threshold dependence, the eigenvalue ϵ_0 is the critical parameter that determines the magnitude of the population loss due to the time-dependent magnetic field. Aside from determining this energy, the detailed form of the trapping potential plays only a secondary role in the dynamics.

Equation (28) also defines a finite set of vibrational states with negative eigenvalues $\epsilon_v<0$. These are the true dimer bound states defined by U_{bg} and will be labeled in descending order with negative vibrational quantum numbers $v<0$. Thus the $v=-1$ level approximates the highest bound state supported by the $a\,^3\Sigma_u^+$ potential.

We have taken two forms for U_{trap}. We first assume that each trapped atom $i=1$ and 2 of mass m experiences an harmonic confining potential $U_{trap}(R_i)=m\omega_o^2R_i^2/2$. This might be a reasonable choice for atoms tightly confined in an optical lattice [10,11], or for a low-density atom trap before the atoms become condensed. It is an especially attractive choice because, for two identical atoms of mass m confined in a spherically harmonic trap, the Hamiltonian transformed into center of mass $\vec{R}_{cm}=(\vec{R}_1+\vec{R}_2)/2$ and relative coordinates $\vec{R}=\vec{R}_2-\vec{R}_1$ is separable:

$$\left(T_{\vec{R}_1}+\frac{1}{2}m\omega_oR_1^2\right)+\left(T_{\vec{R}_2}+\frac{1}{2}m\omega_oR_2^2\right)\equiv\left(T_{\vec{R}_{cm}}+\frac{1}{2}M\omega_oR_{cm}^2\right)+\left(T_{\vec{R}}+\frac{1}{2}\mu\omega_oR^2\right), \tag{29}$$

where $M=2m$, $\mu=m/2$, and $T_{\vec{x}}$ is the three-dimensional (3D) kinetic energy operator. Equation (29) shows that $U_{trap}(R)=\mu\omega_o^2R^2/2$. For nonspherical traps [7,8] we can use the mean trapping frequency $\omega_0=\sqrt[3]{\omega_X\omega_Y\omega_Z}$. The 3D harmonic-oscillator spectrum for the $l=0$ state of relative motion is

$$\epsilon_v=\hbar\omega_o\left[\frac{3}{2}+2v\right]. \tag{30}$$

These eigenvalues are only slightly shifted when the interaction potential U_{bg} is taken into account. Figure 5 schemati-

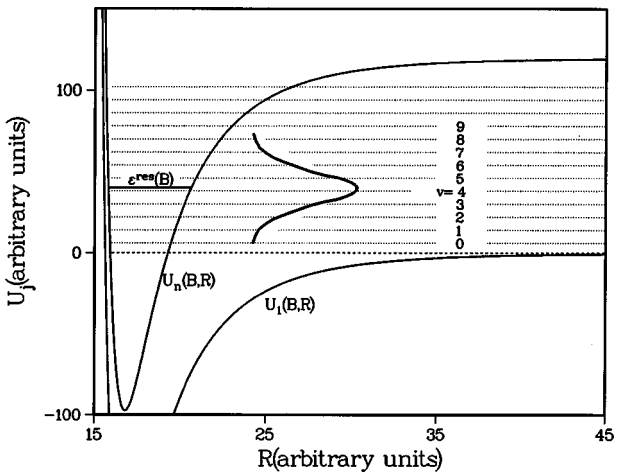

FIG. 5. Schematic diagram of the spectrum defined by $U_{bg}=U_{bg}+U_{trap}$ in Eq. (28) and the resonance energy $\epsilon_n^{res}(B)$ of the vibrational state ϕ_n^{res} supported by the potential U_n. The location of the resonance is a function of B. The bell-shaped curve schematically represents the squared resonance state contributions $|A_n(B,\epsilon_d)|^2$ for multichannel eigenfunctions, with energy ϵ_d in the vicinity of ϵ_n^{res}.

cally represents these trapped state eigenvalues for the harmonic-potential solutions of Eq. (28).

Our second choice is a spherical box potential [23],

$$U_{trap}(R)=\begin{cases}0 & \text{for } R<L\\ \infty & \text{for } R>L.\end{cases} \tag{31}$$

The $l=0$ spectrum for a box potential is

$$\epsilon_v=\frac{\hbar^2\pi^2}{2\mu L^2}(v+1)^2. \tag{32}$$

Again, for the traps we shall consider, the actual eigenvalues are slightly shifted when U_{bg} is taken into account. This box simulates a confined collision in the presence of a finite-sized Bose-Einstein condensate where the size L roughly approximates the dimension of the condensate wave function. In fact we determine L by requiring that ϵ_0 equal the mean kinetic energy of a colliding pair of atoms in the condensate. The exact fitting procedure, discussed in Sec. V and the Appendix, follows from an extension of the Thomas-Fermi model [22].

B. Trapped-state CI model and coupling matrix elements

The configuration-interaction model of Sec. II B is modified due to the presence of a trapping potential in the open channel $|1,\mathrm{CI}\rangle$. We introduce the trapping into the CI model by replacing the radial function F_1 in Eq. (9) with a summation over the complete set of vibrational states ϕ_v supported by Eq. (28), i.e.,

$$\Psi_n(\epsilon_d,B)=|1,\mathrm{CI}\rangle\sum_v \phi_v(R)C_v(\epsilon_d) + |n(B)\rangle\phi_n^{res}(R)A_n(\epsilon_d,B). \tag{33}$$

The coefficients $C_v(\epsilon_d)$ and $A_n(\epsilon_d,B)$ are obtained by inserting Eq. (33) into Eq. (12), where $U_{bg}(R)$ is replaced by $\overline{U}_{bg}(R)$ and solving the resulting matrix eigenvalue problem. The ϵ_d's are eigenenergies belonging to the multichannel eigenfunctions $\Psi_n(\epsilon_d,B)$, which for a fixed B form a discrete set of states.

Solving for the multichannel trapped states requires the evaluation of the coupling matrix element $V_{n,v}(B)$ between the isolated resonance state $|n\rangle\phi_n^{res}$ and the trapped state $|1,\mathrm{CI}\rangle\phi_v$:

$$V_{n,v}=\langle\phi_n^{res}|W_{n,1}(R)|\phi_v\rangle. \tag{34}$$

Using the relation [33,34]

$$\langle\phi_n^{res}|W_{n,1}(R)|\phi_v\rangle\sqrt{\frac{\partial v}{\partial\epsilon_v}}=\langle\phi_n^{res}|W_{n,1}(R)|\phi_\epsilon\rangle \tag{35}$$

between bound-bound and bound-free matrix elements, where $\partial v/\partial\epsilon_v$ measures the density of trapped states in the vicinity of $\epsilon_v\approx\epsilon_n^{res}$, we can relate $V_{n,v}$ to the width $\Gamma_n(\epsilon)$ in Eq. (21):

$$2\pi V_{n,v}^2=\Gamma_n(\epsilon_v)\frac{\partial\epsilon_v}{\partial v}. \tag{36}$$

The exact position $\epsilon_n^{res}(B)$ of the resonant vibrational level, determined by the reference potential $U_n(B,R)$ in Eq. (18), shifts linearly with B as prescribed by Eq. (19). As long as B is such that ϵ_n^{res} is well removed from threshold, we can expect the distribution of resonance state amplitudes $|A_n(\epsilon_d,B)|^2$ for eigenvalues ϵ_d in the vicinity of ϵ_n^{res} to mimic a discretized version of the Lorentzian line shape in Eq. (25). This feature is sketched in Fig. 5.

Using the interaction $W_{n,1}(R)$ defined in Eq. (22), we explicitly evaluate $V_{n,v}$ by using in Eq. (34) the numerical solutions to the CI model. This allows us to rigorously treat all v levels, including those near threshold and even below threshold where the true bound states exist. Using Eqs. (34)–(36) and the threshold properties of Eqs. (23) and (24), we predict the following threshold energy dependence:

$$V_{n,v}=\mathrm{const}\times\sqrt[4]{\epsilon_v}\ \sqrt{\frac{\partial\epsilon_v}{\partial v}}. \tag{37}$$

This predicted variation is confirmed by our numerical calculations for both the harmonic and box trapping potentials.

Since $\partial\epsilon_v/\partial v=2\hbar\omega_o$ is independent of ϵ_v for the spherical harmonic trap, $V_{n,v}$ approaches threshold as $\sqrt[4]{\epsilon_v}$. The magnitude of the coupling varies as $\omega_o^{3/4}$ for a trapped level with $v\geqslant 0$. Noting that the characteristic scale length $l_o=\sqrt{\hbar/\mu\omega_o}$ of a harmonic trapping potential varies at $\omega_o^{-1/2}$, we find that $V_{n,v}$ is proportional to $l_o^{-3/2}$ and is inversely proportional to the square root of the volume of the trap.

An additional $\sqrt{[}4\epsilon_v$ energy dependence is obtained from the density of states factor for the spherical-box potential

$$\sqrt{\frac{\partial \epsilon_v}{\partial v}} = \sqrt[4]{\frac{2\epsilon_v \hbar^2 \pi^2}{\mu L^2}}, \tag{38}$$

and in this case $V_{n,v}$ approaches threshold as $\sqrt{\epsilon_v}$. Nevertheless, for a given $v \geqslant 0$ the coupling matrix element $V_{s,v}$ varies as $L^{-3/2}$, and also scales inversely with the square root of the volume of the confining potential. In fact, as long the volume of the condensate is correctly introduced into the calculations by choosing either L or ω_o to yield the proper trapped-state eigenvalue ϵ_0 in Eq. (37), the condensate modeling will be insensitive, to within a factor of 1.5 due to a difference in the $v=0$ density of states, to the exact form we take for the trapping potential.

IV. TIME DEPENDENT CI MODEL OF FESHBACH RESONANCES

We convert the CI wave function [Eq. (33)] into a time-dependent form by taking

$$B(t) = \begin{cases} B_o, & t < 0 \\ B_o + \dfrac{\partial B}{\partial t} t, & t \geqslant 0, \end{cases} \tag{39}$$

such that

$$H_n(t) = \begin{cases} H_n(B_o), & t < 0 \\ H_n(B_o) + \dfrac{\partial \epsilon_n^{res}}{\partial B} \dfrac{\partial B}{\partial t} t, & t \geqslant 0. \end{cases} \tag{40}$$

We assume that the population initially resides in the trapped vibrational state $v=i$ which imposes the initial condition

$$\Psi_n(t) = |1,CI\rangle \phi_i \quad t \leqslant 0. \tag{41}$$

In particular we are interested in the case $i=0$. The initial B_o is chosen such that the resonance position $\epsilon_n^{res}(B_o)$ is well removed from the vicinity of the threshold. If B_o is not sufficiently removed from the threshold, then it is imperative to use an initial state which is properly ''dressed'' by the initial magnetic field. This corresponds to choosing an eigenstate $\Psi_n(\epsilon_d, B)$ of the Hamiltonian $H(B_o)$ in Eq. (33). The proper choice of initial state is dictated by how the initial state was prepared in a particular experiment. For example, we implicitly assume that the system was slowly and adiabatically brought to its $t=0$ condition.

The coefficients in Eq. (33) are now time dependent,

$$\Psi_n(t) = |1\rangle \sum_v \phi_v(R) C_v(t) + |n(t)\rangle \phi_n^{res}(R) A_n(t), \tag{42}$$

and must satisfy the time-dependent Schrödinger equation

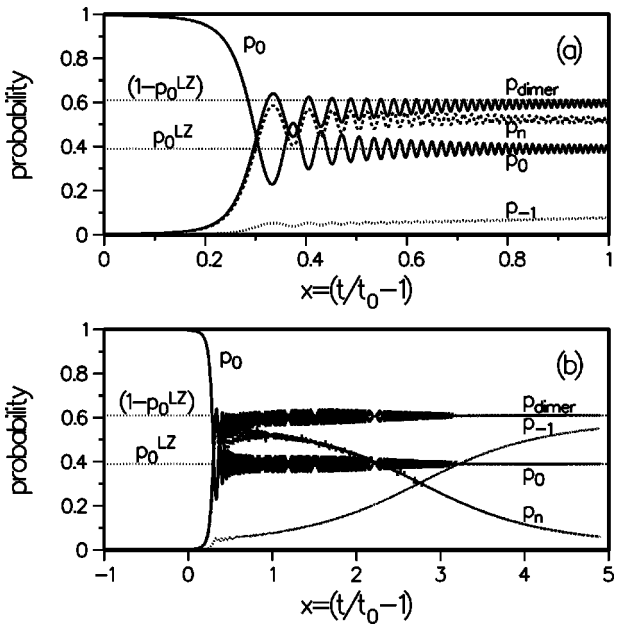

FIG. 6. (a) Population density for negative ramp rate -0.76 T/ms where the resonance crosses the initial harmonic trap state $i=0$ from above and $\omega_o/2\pi = 1$ MHz. Choosing $t_0 = 2$ μs, the initial ϵ_n^{res}/k_B position is 3.8 mK above threshold and crosses the initial $i=0$ state at $x \approx 0$. The 61% depletion of p_0 is exactly given by Landau-Zener probability p_0^{LZ}. This loss $(1-p_0) = p_n + p_{-1}$ leads to the formation of *stable dimer molecules*. After crossing the threshold the population is predominantly in the resonance state p_n, which now represents a true bound state of the dimer. (b) The expanded time scale shows the population as the resonance crosses the highest vibrational state $v=-1$ in potential U_1, and the population p_n is switched to p_{-1}.

$$i\hbar \frac{\partial \Psi_n(t)}{\partial t} = H_n(B(t)) \Psi_n(t). \tag{43}$$

Given the coupling matrix elements $V_{n,v}$, which we evaluate numerically for a finite, but large, set of vibrational levels, we can easily solve the set of linear first-order equations

$$i\hbar \dot{A}_n = \left[\epsilon_n^{res}(B_o) + \frac{\partial \epsilon_n^{res}}{\partial B} \frac{\partial B}{\partial t} t \right] A_n + \sum_v V_{n,v} C_v, \tag{44}$$

$$i\hbar \dot{C}_v = [\epsilon_v] C_v + V_{n,v} A_n \tag{45}$$

for the coefficients $A_n(t)$ and $C_v(t)$ using a standard numerical algorithm. We have carefully checked the convergence of the results to insure they are independent of the size of the vibrational basis.

A. Dimer formation in a harmonic trap

An example of our numerical results is shown in Fig. 6, where we start the system at $t=0$ in the lowest harmonic state $|1\rangle \phi_o$ with $\omega_o/2\pi = 1$ MHz, $l_o = 561 a_o$, and $\epsilon_o/k_B = 78.4$ μK. With an initial field $B_o \approx 92.5$ mT the resonance state is located at $\epsilon_n^{res}(B_o)/k_B \approx 3.8$ mK, and is far enough above threshold that the interaction with the lowest trap state

is negligible. The field is then ramped *downward* at a rate $\partial B/\partial t = -0.76$ T/ms, such that the resonance energy position $\epsilon_n(B_n^{res})$ coincides with the eigenvalue of the initial state $\epsilon_{i=0}$ at $t_n \approx 2$ μs, i.e.,

$$t_n = [B_n^{res} - B_o]\frac{\partial t}{\partial B}. \tag{46}$$

Shortly after passing ϵ_0 at $t = t_n$ the resonance sweeps past threshold at which time $\epsilon_n^{res}(B)$ becomes negative and the resonance state represents a *true bound state* of the dimer.

The probability of being in a specific vibrational state ϕ_v associated with the open channel $|1,\mathrm{CI}\rangle$ is given by $p_v(t) = |C_v(t)|^2$, while the probability that the population is transferred into the passing resonance state is given by $p_n(t) = |A_n(t)|^2$. The various populations are plotted in Fig. 6 versus the dimensionless quantity $x = (t/t_n - 1)$, where $x = 0$ coincides with the crossing of the resonance and the initial bound state (passage across threshold occurs at $x = 0.005$). Initially $p_0(0) = 1$, and all other probabilities are zero. As we pass $x = 0$ and the resonance state is dragged well below threshold by the decreasing magnetic field we find in this case that 61% of the initial population is lost. Initially this population is mostly transferred to p_n, implying that the loss is due to the *formation of stable dimer molecules* in the state $|n(t)\rangle\phi_n^{res}(R)$. Moreover, a small amount of population begins to appears in p_{-1}, which is also a stable state of the dimer corresponding to the very last bound state supported by the open-channel potential $U_{bg}(R)$.

Our numerical calculations show that the probability of remaining in the initial state $|1\rangle\phi_i$ as $t \to \infty$ is given by the Landau-Zener expression [24]

$$p_i(t \to +\infty) \equiv p_i^{LZ} = \exp(-w_{n,i}^{LZ}), \tag{47}$$

where

$$w_{n,i}^{LZ} = \frac{2\pi |V_{n,i}|^2}{\hbar \left| \dfrac{\partial \epsilon_n^{res}}{\partial B}\dfrac{\partial B}{\partial t} \right|}. \tag{48}$$

This agreement is demonstrated in Fig. 6 for $i = 0$, and is found to work equally well for the depletion of any initial state which is crossed by the time-dependent resonance state. Although the LZ theory only predicts the *asymptotic* probability when the resonance is sufficiently distant that it no longer interacts with the initial state, we see that the loss occurs over a finite time interval, and is essentially complete by $x \approx 0.5$.

If the sweeping field is stopped at say, $x = +1$, as in Fig. 6(a), the total loss

$$p_{loss}(i) = 1 - p_i^{LZ} = 1 - \exp(-w_{n,i}^{LZ}) \tag{49}$$

primarily contributes to the resonance state population $p_n \approx p_{loss}(0)$, with a small quantity appearing in p_{-1}. Of course if we continue sweeping the magnetic field downward the resonance will eventually cross the bound vibrational state $v = -1$, and we then find that population is transferred from p_n to p_{-1}. Again, as demonstrated in Fig. 6(b), this transfer is given by the LZ theory, i.e, $p_n = p_{loss}(0)p_{-1}^{LZ}$ and $p_{-1} = p_{loss}(0)(1 - p_{-1}^{LZ})$. The probability $p_{-1}^{LZ} = \exp(-w_{n,-1}^{LZ})$ is obtained from Eq. (48) with $V_{n,-1}$ replacing $V_{n,0}$. Since the $V_{n,-1}$ coupling is two orders of magnitude larger than $V_{n,0}$, we find that $p_{-1}^{LZ} \approx 0$. This means the $n \leftrightarrow v = -1$ crossing is essentially 100% adiabatic with $p_n \approx 0$ and all the lost population is transferred to $p_{-1} \approx p_{loss}(0)$.

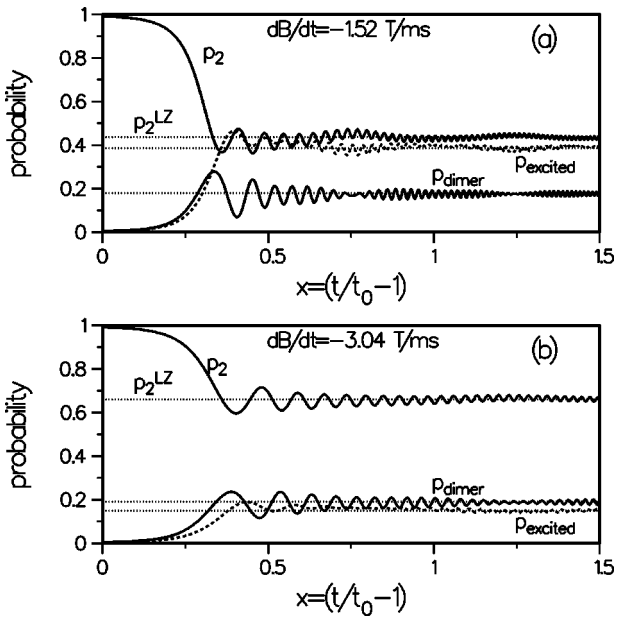

FIG. 7. (a) Population density for a negative ramp rate of -1.52 T/ms with the resonance crossing the initially populated harmonic trap state $i = 2$ from above. (b) Same as (a) but with a ramp rate of -3.04 T/ms.

Let us denote the total population of dimer molecules, regardless of their internal state as follows:

$$p_{dimer} = p_n + \sum_{v<0} p_v. \tag{50}$$

We also define $p_{excited}$ as the total population of harmonic trap states that has been removed from the initial state,

$$p_{excited} = \sum_{v \geq 0} p_v - p_i, \tag{51}$$

such that $p_i + p_{dimer} + p_{excited} \equiv 1$. In this instance, since we are starting from $i = 0$, this means that $p_{dimer} \approx p_{loss}(i)$ and $p_{excited} \approx 0$. These equalities are demonstrated nicely in Fig. 6. Note that by manipulating the ramp rate of the applied magnetic field we can control the formation of the alkali dimers. At very slow ramp rates Eq. (49) predicts that essentially 100% of the population is transferred from p_0 to p_n, and then to p_{-1}. In this scenario $p_{dimer} = p_{loss}(i) = 1$ and the entire initial trapped population can be transformed to vibrationally hot, but translationally and rotationally ultracold dimers.

Figure 7 illustrates the case of starting from a higher ini-

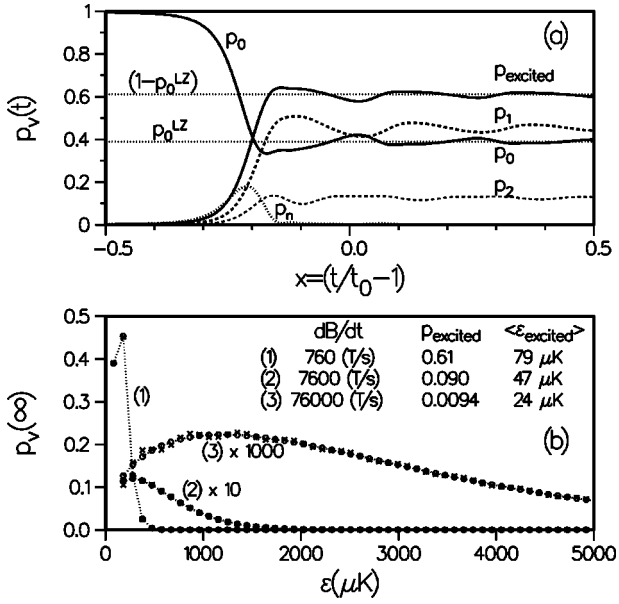

FIG. 8. (a) Population density for a ramp rate of +0.76 T/ms and $\omega_o/2\pi=1$ MHz, where the resonance crosses the initial harmonic trap state $i=0$ from below, starting from −3.8 mK. An identical amount of population is lost as in Fig. 6, and is again exactly given by p_0^{LZ}. In this case the lost population is deposited into vibrationally excited trap states $v>0$, with the detailed distribution in agreement with the generalized LZ expression in Eq. (53). (b) Comparison of exact and Landau-Zener distributions of harmonic trap states for $v>i$ excited by three different positive ramp rates.

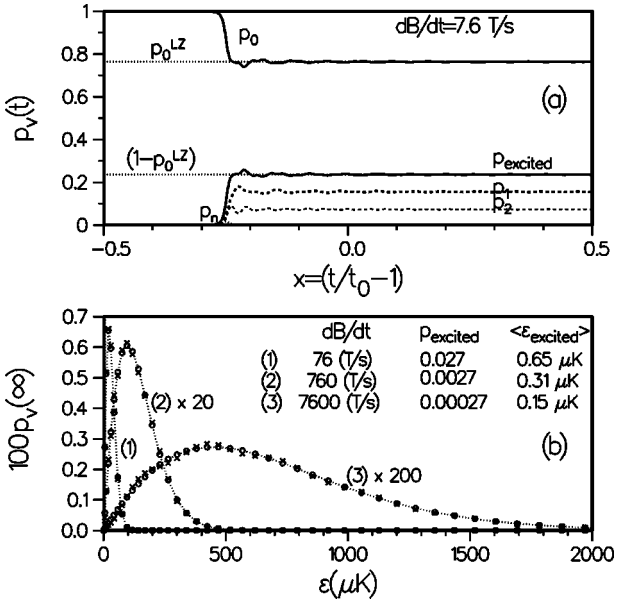

FIG. 9. (a) Population density for a ramp rate of +0.76 T/ms, where the resonance crosses the initial spherical box trap state $i=0$ from below, starting from −3.8 mK ($L=8000a_o$). The lost population is deposited into vibrationally excited trap states $v>0$, with the detailed distribution in agreement with the generalized LZ expression in Eq. (53). (b) Comparison of exact and Landau-Zener distributions of box trap states for $v>i$ excited by three different positive ramp rates ($L=8000a_o$).

tial harmonic state, such as $i=2$. The lost population $p_{loss}(2)$ is distributed between the trapped states $p_{excited}$ with $0\leqslant v<i$ and the true dimer states p_{dimer}. We find agreement with the predictions of multiple crossing Landau-Zener theory for $v<i$,

$$p_v(+\infty)\approx p_{loss}(i)p_{i-1}^{LZ}p_{i-2}^{LZ}\cdots p_{v-1}^{LZ}(1-p_v^{LZ}). \quad (52)$$

B. Excitation of trapped-state populations

For the case shown in Fig. 8, we reverse the procedure in Fig. 5 and start with the resonance located at the same distance *below threshold*, and ramp the field *upward* at the rate $\partial B/\partial t=+0.76$ T/ms. Again we start in the initial state $i=0$, but now with an initial magnetic field $B_o\approx 89.5$ mT which locates the resonance state at $\epsilon_n(B_o)/k_B\approx -3.82$ mK and yields the same crossing time t_n in Eq. (46). The resonance lies between the last bound state $v=-1$ and the threshold, and far enough removed that the initial interaction with the lowest trap state is negligible.

As the magnetic field sweeps upward the resonance crosses the initial state $i=0$ at $x=0$. By the time the resonance reaches $x\approx 0.5$ it has crossed 20 trap states and any population it acquired in crossing $i=0$ has been lost along the way. As implied by $p_n\to 0$ and the definitions in Eqs. (50) and (51), all the population lost from $i=0$ resides in excited vibrational levels, i.e., $p_{excited}=p_{loss}(0)$. Again, we find the distribution amongst the individual vibrational states is exactly given by the multiple-crossing LZ theory [25,26] for $\partial B/\partial t>0$ and $v>i$,

$$p_v(+\infty)=p_{loss}(i)p_{i+1}^{LZ}p_{i+2}^{LZ}\cdots p_{v-1}^{LZ}(1-p_v^{LZ}). \quad (53)$$

The success of Eq. (53) is amply demonstrated in Fig. 8(b), where we show the complete excited state distributions for three different ramp rates $\partial B/\partial t$. The total loss rates $p_{loss}(i)$ equals $p_{excited}$ listed in Fig. 8(b) and scale perfectly according to Eqs. (49), (48), and (53). The individual LZ probabilities map the exact numerical results to within a few percent for $p_v>10^{-7}$, and small deviations are probably due to numerical inaccuracies in our calculations. The table in Fig. 8(b) shows how $p_{excited}$ decreases with the inverse ramp rate $\partial t/\partial B$, becoming proportional to it as it becomes smaller. It is interesting to note that when the ramp rate is increased the smaller amount of population that is transferred from the initial state to the resonance is ultimately deposited into significantly higher vibrational states. Therefore, as seen in the Fig. 8(b), the mean amount of vibrational energy delivered to the system,

$$\langle\epsilon_{excited}\rangle=\sum_{v>i}\epsilon_v p_v, \quad (54)$$

has a much slower dependence on the inverse ramp rate than $p_{excited}$.

Figure 9 demonstrates that we obtain exactly the same behavior, and the same excellent agreement with the LZ theory if we use a box trapping potential in place of the

harmonic potential. In this case we have substantially increased the density of states by using $L=8000a_o\approx 0.4\ \mu$m in Eq. (32), such that $\epsilon_{i=0}/k_B=1.172\ \mu$K. We also use slower ramp rates and the loss in now perfectly linear in $\partial t/\partial B$. Again the mean amount of energy deposited into the excited harmonic trap states decreases much more gradually than $p_{excited}$.

C. Landau-Zener parameters for Na resonances

Our numerical calculations have demonstrated that the LZ expressions are essentially exact. The largest L we could comfortably handle in our exact time-dependent calculations was the $L=8000a_o$ used to obtain the results in Fig. 9. Since we will need much larger L values in Sec. V, here we give simple expressions for evaluating the LZ loss rates for the two Na resonances in arbitrary size traps. These LZ expressions can be used with confidence to predict the magnetic-field response for cases where explicit numerical solutions to Eqs. (44) and (45) are impractical.

Using the CI parameters deduced in Sec. II B 3 to reproduce the strong $\Gamma_s=350\ \mu$K resonance located at $\epsilon_s^{res}=1300\ \mu$K for $B=91.5$ mT in Fig. 4(a), we obtain the following bound-state coupling matrix element for $v\geqslant 0$:

$$V_{s,v}(\mu\mathrm{K})=177.0\sqrt{\frac{\epsilon_v(\mu\ \mathrm{K})}{L(a_o)}}=1.526\times 10^6\frac{(v+1)}{[L(a_o)]^{3/2}}, \tag{55}$$

where the units needed are indicated in parentheses. We have confirmed this formula by numerical examples. Introducing expression (55) into Eq. (48), and using Eq. (8), we predict

$$\omega_{s,v}^{LZ}=\frac{1.11\times 10^{-10}(v+1)^2}{[L(\mathrm{cm})]^3}\left|\frac{\partial t(\mathrm{s})}{\partial B(\mathrm{mT})}\right|. \tag{56}$$

A similar fitting for the weak $B=86.15$ mT resonance in Fig. 4(b) using $\Gamma_w=2.95\ \mu$T at $\epsilon_w^{res}=953.4\ \mu$K yields a LZ probability which is two orders of magnitude smaller:

$$\omega_{w,v}^{LZ}=0.0095\omega_{s,v}^{LZ}. \tag{57}$$

It is interesting to note that the LZ probability predicted using the 3D harmonic trapping potential in place of spherical box potential has a similar functional dependence to those of Eqs. (56) and (57), with the characteristic harmonic length parameter $l_o=\sqrt{\hbar/(\mu\omega_o)}$ replacing L:

$$\omega_{s,v}^{LZ}(\mathrm{harmonic})=\frac{1.27\times 10^{-11}\left(1+\frac{4}{3}v\right)}{[l_o(\mathrm{cm})]^3}\left|\frac{\partial t(\mathrm{s})}{\partial B(\mathrm{mT})}\right|. \tag{58}$$

The same functional form is obtained for the weak resonance with the coefficient reduced to 1.20×10^{-12}. Note that if we choose $l_o\equiv\sqrt{3}L/\pi$, which insures that harmonic and box traps both yield identical trapped state eigenvalues ϵ_0, the LZ probabilities in Eqs. (56) and (58) only differ by a factor of 1.5 due to the difference in the density of vibrational states $\partial\epsilon_v/\partial v$.

V. APPLICATION OF FESHBACH MODEL TO MIT EXPERIMENTS

A. Ramp of resonance through threshold

It would not be realistic to represent the trapping potential in the case of a Na BEC as a harmonic one. The reason for this is that atom-atom interactions cause the condensate wave function to expand and to occupy a volume many times that of the ground state of the harmonic oscillator, and to have a much lower kinetic energy than $\frac{3}{2}\hbar\omega_o$. This expansion modifies the properties of the threshold matrix element, which scales with L as described in Sec. IV C. As discussed in the Appendix, we propose to represent the trapping potential in a BEC formed in a harmonic trap of mean frequency ω_o by the spherical-box potential in Eq. (31) with radius L. This form is suggested by the simple Thomas-Fermi solution to the Gross-Pitaevskii equation, for which the condensate atoms move in a flat effective potential inside the Thomas-Fermi radius. Although the mean kinetic energy between a pair of interacting atoms is zero in this approximation, Fetter and Feder [36] derived an expression for the finite mean kinetic energy $\langle T\rangle$ of a condensate atom. Furthermore, the lowest trapped state $v=0$ is occupied in a condensate. By requiring that the ground-state energy $\epsilon_0=\hbar^2\pi^2/2\mu L^2$ of the atom pair in the spherical box be identical to the mean kinetic energy of an atom in the condensate, we *choose* L to insure that $\epsilon_0\equiv\langle T\rangle$. The Appendix shows that for the MIT experiments $L\approx 10\ \mu$m and $\epsilon_o\approx 2.1$ nK.

The $B(t)$ ramp in the experiment [8] moves the resonance from below to above threshold, and we assume that atoms removed from the ground state and placed in trapped states with $i\geqslant 1$ are lost from the condensate. In essence, heating the atoms leads to atom loss. For this experiment the LZ parameter $\omega_{n,0}^{LZ}$ is very small, only on the order of 10^{-6}, so that

$$p_{loss}(n,i=0)=1-e^{-\omega_{n,0}^{LZ}}\approx\omega_{n,0}^{LZ}. \tag{59}$$

This is the probability that a *particular atom* interacting with *one* of the other atoms in the condensate will experience a loss as the field ramps the resonance across threshold. However, there are $N-2\approx N$ additional atoms with which the atom can simultaneously and, assuming that three-body interactions can be neglected, independently experience resonance interaction. Thus the total probability that the Feshbach resonance extracts this particular atom from the ground state of the condensate is enhanced by a factor of N, such that

$$P_{loss}^{total}(n,0)=1-e^{-N\times\omega_{n,0}^{LZ}}. \tag{60}$$

If $N\times\omega_{n,0}^{LZ}$ becomes large the exponential form insures that Eq. (60) maintains unitarity. Using Eqs. (56) and (57), the fraction of condensate atoms that are lost from the initial box state $i=0$ is

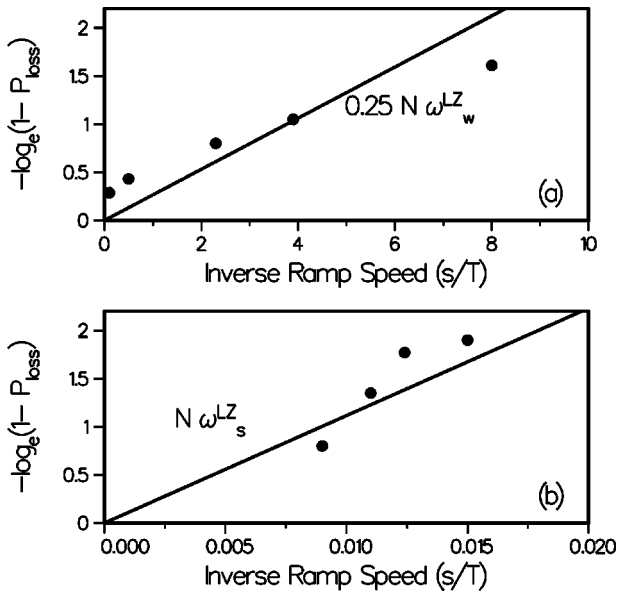

FIG. 10. Comparison of the calculated LZ probability $N\times\omega^{LZ}(i)$ vs the observed quantity $-\ln(1-P_{loss})$ from Ref. [8] for both weak and strong resonances. A factor of 0.25 for $\omega_w^{LZ}(i)$ corrects the calculated resonant width to agree with the measured one for the weak resonance, and brings the calculated and observed losses into good agreement.

$$P_{loss}^{total}(n,0)\approx 1-\exp\left(-\alpha(n,0)\rho_b\left|\frac{\partial t(\mathrm{s})}{\partial B(\mathrm{mT})}\right|\right), \qquad (61)$$

where $\rho_b=N/[L(\mathrm{cm})]^3$ is proportional to the mean atom density ρ_A of the condensate. This proportionality to mean density is a consequence of the inverse volume dependence of $\omega_n^{LZ},0$ in Eq. (56). We find $\alpha(s,0)=1.11\times10^{-10}$ for the strong resonance and $\alpha(w,0)=1.06\times10^{-12}$ for the weak resonance.

In order to compare the loss predicted by Eq. (61) with the observed loss [7,8], it is necessary to know N, and to specify the scaling parameter L. The former was measured, and the latter was obtained as described in the Appendix. We find that Eq. (61) predicts fractional losses of atomic population from state $i=0$ for the two observed resonances that are consistent with the magnitudes of the losses found in the experiments. For instance, from the data in Fig. 3 of Ref. [8], it is observed that 70% of the atoms are lost from the condensate at inverse ramp rates of 10 and 4000 μs/mT for the strong (90.7 mT) and weak (85.3 mT) resonances, respectively. Our results using the measured $N=9\times10^5$ predict losses of 63% and 98% for these respective resonances. However, our calculated width Γ_w is roughly a factor of 4 larger than that inferred from the experiment. Reducing $\alpha(w,0)$ by a factor of 4 reduces the weak resonance loss from 98% to 63%, in good agreement with the observations. Comparable agreement was found for the case given in Ref. [7].

Figure 10 compares $N\times\omega_{n,0}^{LZ}$ with the experimental points for $-\ln(1-P_{loss})$, found from P_{loss} reported in Fig. 3 of Ref. [8]. Since our theoretical calculations contain no arbitrary fitting parameters, the fact that Eq. (61) gives generally good agreement for the observed loss rates is very satisfying, and strongly recommends this ramping mechanism as a possible source of the unexplained losses in the experiment.

B. Resonance stabilization by a third body

The MIT experiments also observed large atom losses when a magnetic field very slowly moves a Feshbach resonance near to but not through the threshold region. Timmermans *et al.* [12] and Yurovsky *et al.* [13] already proposed another possible loss mechanism for this case, namely, the quasibound resonance state that introduces the resonance structure strongly enhances the three-body recombination. A collision with a third Na atom causes a vibrational relaxation of the resonant state $\mathrm{Na}_2(n)$ to form a stable dimer $\mathrm{Na}_2(d)$, i.e., $\mathrm{Na}_2(n)+\mathrm{Na}\rightarrow\mathrm{Na}_2(d)+\mathrm{Na}+\Delta E$, with the excess energy ΔE added to the kinetic energy of the atom and the dimer. This vibrational relaxation is characterized by a binary rate constant $\gamma_d(\mathrm{cm}^3/\mathrm{s})$. Although this model was developed using a coupled Gross-Pitaevskii formalism, it is equally well described in a microscopic scattering approach as a resonance-enhanced three-body recombination mechanism with a cross section given by the usual Breit-Wigner expression [27],

$$\sigma(d)=\frac{\pi}{k^2}\frac{\Gamma_n\Gamma_d}{(\epsilon-\epsilon_n^{res})^2+(\Gamma_n+\Gamma_d)^2/4}. \qquad (62)$$

The partial width $\Gamma_d(\epsilon)=\hbar\gamma_d\rho_A$ for converting a quasibound resonance state into the bound state d is proportional to the atom density ρ_A. Dimer formation and the release of kinetic energy would lead to significant loss of trapped atoms. This model may very well give the proper explanation of the experiments where the magnetic field is slowly brought close to resonance and then held fixed, although in Ref. [13] the energy-transfer rate γ_d is introduced as an adjustable parameter and remains to be justified. In the Wigner threshold region the vibrational relaxation width Γ_d will approach a constant, while Γ_n exhibits the expected $\sqrt{\epsilon}$ threshold dependence.

If we introduce a complex resonance position $\epsilon_n^{res}(B_o)+i\Gamma_d/2$ into Eq. (44), then this resonance stabilization mechanism can be introduced into our formalism as a loss process represented by the complex potential $i\Gamma_d/2$. Although we have not explicitly carried out such calculations, the LZ theory predicts that the total loss of population from the initial trapped state ϵ_i due to a magnetic field ramp $B(t)$ is still given by Eqs. (47) and (48). If Γ_d is sufficiently large compared to Γ_n, then the population is transferred to the stable dimer state d via a three-body collision instead of being moved to other levels due to nonconservative interactions with the time-dependent magnetic field.

We note that Eq. (62) is equivalent to the standard expression for trap loss due to photoassociation. This process may be viewed in a dressed-molecule picture as optically coupling the ground scattering continuum to an optically tunable excited state Feshbach resonance level that decays by spontaneous emission [38]. In this case, the photon plays the role of the third body that causes the loss process, and the spon-

taneous emission width replaces Γ_d in Eq. (62). Our CI theory could also be applied to photoassociation viewed as an optically induced Feshbach resonance process. An analog to molecule formation via a $B(t)$ ramp of a Feshbach resonance is a recent proposal to make cold molecules efficiently by frequency-chirped photoassociation [15].

VI. DISCUSSION AND CONCLUSIONS

We have carried out a study of the Feshbach resonances for the collision of two Na atoms in the lowest $f=1,m=+1$ ground-state hyperfine level in a time-dependent magnetic field $B(t)$. The theory gives a rigorous account of the dynamics induced by $B(t)$ for two atoms initially confined in the ground state of a 3D harmonic trap. Although our calculations are for Na atoms, the methodology is general and can be extended to any pair of alkali atoms of the same or different species. We envision applications to a variety of trapping situations, but specifically apply our results to interpret recent experiments with a Na BEC.

We start with a rigorous close-coupled formulation of the two-body collision, and end with a remarkably simple Landau-Zener time-dependent curve-crossing model for the dynamics of atoms in discrete energy levels in a trap. The bridge between the contrasting scattering and trap viewpoints is facilitated by a two-channel CI theory, which gives a simple parametrization of an isolated Feshbach resonance interacting with the continuum states of the colliding atoms. The key parameters are a tunable resonance position $\epsilon_n^{res}(B)$ and a resonance width Γ_n. The CI theory was set up within the standard time-independent scattering viewpoint, where the resonance level n is a bound state embedded in a scattering continuum where the asymptotically free particles separate with relative kinetic energy $\epsilon>0$. We adapt the theory to the case of trapped atoms which experience a confining potential at large interatomic separations R. In this case, there is a discrete set of eigenstates i with eigenenergies $\epsilon_i>0$ instead of a continuum of states, and the coupling between the resonance and these discrete levels is given by a matrix element $V_{n,i}$, which is related to Γ_n.

A time-dependent B field shifts the energy position of the resonance relative to the energy ϵ_i of the initially prepared level i of the trapped atoms, thereby inducing transitions for which we calculate the probability. We are especially interested in the case where i represents the ground state of the trap, $i=0$. When a ramp of $B(t)$ sweeps the resonance position $\epsilon_n^{res}(B)$ past ϵ_i, population transfers from level i to the resonance level n. If $\epsilon_n^{res}(B)$ starts below ϵ_i, the resonance is carried into the ''quasicontinuum'' of discrete trapped states, and it deposits its energy in excited trapped states. By contrast, if $\epsilon_n^{res}(B)$ starts above ϵ_i, the $B(t)$ ramp carries the resonance position below threshold where it now represents a stable (nondecaying) dimer state. If the ramp carries $\epsilon_n^{res}(B)$ across a bound state $i=-1$ of the dimer, population can be transferred to that level as well. A sufficiently slow ramp rate makes any of these transfer processes nearly 100% efficient.

We therefore suggest that a downward ramp will produce stable diatomic molecules which are translationally and rotationally cold, but vibrationally excited, depending of the specific levels available to the atom pair in question. This process might be feasible in optical lattice cells, for example, if two atoms were to occupy the same lattice site. Confinement dimensions significantly less than 0.1 μm should be experimentally possible. There are proposals for bringing two alkali atoms together in the ground state of a single cell of a 3D optical lattice [10,11], and high fractional occupation of lattice sites has recently been demonstrated for a Cs lattice [37]. It is certainly possible that favorable Feshbach resonances might be possible in the Cs system. Molecule production in a Na BEC might also be feasible. However, the expectation of large loss rates of atoms due to collisions with a third atom [13] suggest that inelastic collisional relaxation of the resonance level or of high vibrational levels may prove to be problematical in a condensed system. Such relaxation would not be a problem in an doubly occupied optical lattice cell where there is no third body.

When a ramp of $B(t)$ sweeps the resonance position $\epsilon_n^{res}(B)$ past ϵ_i, the time-dependent field induces population changes in the levels. The probability $p_{loss}(n,i)$ of population loss from an initially populated trap level i is simply explained by a Landau-Zener curve-crossing model, which also accurately gives the distribution of final levels. We can give a simple intuitive interpretation of the expressions in Eqs. (49) or (59) for $p_{loss}(n,i)$. Using the fundamental expression in Eq. (36) which relates $|V_{n,i}|^2$ to the resonance width $\Gamma_n(\epsilon_i)$, the LZ adiabaticity parameter $w_{n,i}^{LZ}$ in Eq. (48) can be expressed as follows:

$$w_{n,i}^{LZ}=\left(\Gamma_n\frac{\partial t}{\partial\epsilon_n^{res}}\right)\left(\frac{\partial\epsilon_i}{\hbar\,\partial i}\right)=(t_{res})(2\pi\nu_i). \tag{63}$$

Here we have written the resonance ramp rate in the simpler form $\partial\epsilon_n^{res}/\partial t$. The first term on the right-hand side of Eq. (63) is clearly the *time in resonance*, that is, the time t_{res} it takes the resonance to ramp over an energy range equal to the width $\Gamma_n(\epsilon_i)$. The second factor in Eq. (63) is the trap spacing divided by $\hbar$, and thus ν_i represents the vibrational frequency of trap level i. Consequently, the LZ adiabaticity parameter $w_{n,i}^{LZ}$ simply equals the resonance time t_{res} times the frequency $2\pi\nu_i$. Thus, if the resonance ramps quickly compared to the vibrational period $1/\nu_i$, then $w_{n,i}^{LZ}\ll 1$, the dynamics is diabatic, and the trap level i remains mostly populated. On the other hand, if the resonance ramps very slowly compared to the vibrational period, $w_{n,i}^{LZ}\gg 1$, the dynamics is adiabatic, and all of the population in i is transferred to the resonance level.

The Wigner threshold law ensures that the width $\Gamma_n(\epsilon_i)$ is proportional to $\sqrt{\epsilon_i}$ [see Eq. (24)]. A trap is characterized by some scale length $L_{\rm scale}$, which is equal to l_o and L for the harmonic and box potentials, respectively. Since in a trap $\sqrt{\epsilon_i}\propto 1/L_{\rm scale}$ and $2\pi\nu_i\propto L_{\rm scale}^{-2}$, we conclude that $w_{n,i}^{LZ}\propto L_{\rm scale}^{-3}$ is inversely proportional to the trap volume. This inverse volume dependence is the manifestation of the Wigner threshold properties for ultracold 3D trapped state dynamics.

The application of our model to a Na BEC leads to remarkably good agreement with the atom losses observed in the MIT experiments with a ramped magnetic field. Our two-body close-coupled model gives excellent agreement with two-body scattering data, including the observed positions of the two Feshbach resonance states (although we differ from experiment by a factor of 4 in the experimentally inferred width of the weaker resonance). The key to applying our model based on binary collisions is to adapt the trapping potential in such a way that the kinetic energy of the colliding atoms is properly represented. This is because the matrix element for the coupling of the resonance to the ground state of the trap depends strongly on the kinetic energy of relative motion. The expansion of the cloud of atoms in the condensate due to the mean-field interaction causes the condensate to have a much lower mean kinetic energy and much larger volume than for the ground state of the harmonic trap. This greatly reduces the coupling matrix element. Using a spherical box potential for which the mean kinetic energy matches the actual mean kinetic energy of the anisotropic condensate permits us to calculate the actual coupling matrix elements and loss rates. Although the LZ probability $w_{n,0}^{LZ}$ for atom loss due to a single pair of atoms in the condensate is quite small, the net probability of atom loss is actually quite large because of the large number of atoms pairs in the condensate. The total loss probability per atom depends on the product $Nw_{n,0}^{LZ}$, which is proportional to the mean atom density because of the above-mentioned scaling of $w_{n,0}^{LZ}$ with inverse volume of the condensate.

The quality of the agreement between predicted and observed losses certainly suggests that the essential physics in our model is correct. Although a similar picture can be obtained using the formalism of coupled atom-molecule Gross-Pitaevskii equations [12–14], we believe that the simple physical model that we have presented will provide much understanding of the role of Feshbach resonances in the BEC context. It also proves to be useful and predictive for other situations which might utilize magnetically controlled atomic collisions, such as molecule formation in lattices or quantum computing [10,11]. There is also a great deal of similarity between magnetically induced Feshbach resonances and optically-induced ones, as we noted at the end of Sec. V B. Two-color photoassociation by stimulated Raman scattering [39] is an example of using optically induced Feshbach resonances for molecule formation in a BEC [40], a process which has recently been studied experimentally [41] and theoretically [42]. Our model should be readily adaptable to the case of condensate photoassociation.

Note added in proof. The work in Ref. [14], which appeared after our paper was submitted, comes to similar conclusions for ^{23}Na BEL Feshbach experiments using an alternative and complementary point of view.

ACKNOWLEDGMENTS

We thank Carl Williams for helpful discussions, and Volodia Yurovsky, Abraham Ben-Reuven, and Eddy Timmermans for providing preprints of their work prior to publication. We also thank the Army Research Office and the Office of Naval Research for partial support.

APPENDIX: ANALYSIS OF CONDENSATE PARAMETERS

Our analysis is based on the work of Fetter and Feder [22], who considered a BEC in an isotropic harmonic trap of frequency ω_o. It was shown by Schneider and Feder [43] that for our purpose the *same* analysis can be applied equally well to an anisotropic trap simply by equating ω_o to the geometric mean frequency $\sqrt[3]{\omega_x\omega_y\omega_z}$. The chemical potential $\mu_A N=\langle T_A\rangle+\langle V_H\rangle+\langle V_{trap}\rangle$ and other properties of an ensemble of N condensate atoms in an isotropic harmonic trap is given by the expectation values of the atomic kinetic energy operator $\langle T_A\rangle$, the mean energy of interaction $\langle V_H\rangle$ which is proportional to the usual scattering length a, and the harmonic trapping potential $\langle V_{trap}\rangle$. These are evaluated using the condensate wave function obtained from the usual Gross-Pitaevskii (GP) equation.

We begin the analysis with the oscillator length for a single trapped atom $d_A=\sqrt{\hbar/(m_A\omega_o)}$. [Note that the oscillator length l_o which we use in Eqs. (64), etc., is for the relative motion of the dimer whose reduced mass equals $m_A/2$ and $l_o\equiv\sqrt{2}d_A$.] The mean volume occupied by the ground state of the harmonic trap is $\langle \upsilon_{harm}\rangle=4\pi d_A^3/3$. The dimensionless parameter $\eta_A=\mathrm{Na}/d_A$ is then used to characterize the strength of the repulsive mean-field interactions introduced by the positive scattering length for the sodium triplet state $a=63.9a_o$. This is related to the dimensionless Thomas-Fermi condensate radius $\Re=(15\eta_A)^{1/5}$, and is a measure of the expansion of the condensate radius due to the mean-field interactions. Thus the mean volume $\langle \upsilon\rangle=4\pi(\Re d_A)^3/3$ of the harmonically trapped condensate is increased by a factor of $\Re^3$ and the mean atom density is $\rho_A=N/\langle \upsilon\rangle$.

The Thomas-Fermi (TF) solution to the GP equation $(T_A+V_H+V_{trap})\Psi(\mathbf{r}_A)=\mu_A\Psi(\mathbf{r}_A)$ is a ''zero'' temperature approximation and involves ignoring the kinetic-energy operator and replacing the potentials V_H+V_{trap} with an effective flat potential $V_{eff}\approx\mu_A$. In the TF limit $\mu_A=\hbar\omega_0\Re^2/2$ and the range of the flat effective potential is of the order of $d_A\Re$.

For a finite radius $\Re$, Fetter and Feder [22] have shown that to next order the expectation value of the kinetic-energy operator is

$$\langle T_A\rangle\approx\frac{5}{2\Re^2}\ln(268\Re)\hbar\omega_o. \tag{A1}$$

This same mean kinetic energy of a condensate atom should correspond to the average relative kinetic energy of two colliding condensate atoms. Since the energy of a spherical box potential is entirely kinetic, it is reasonable to equate the lowest box state eigenvalue in Eq. (30) to the mean kinetic energy of the condensate, i.e., $\epsilon_0\equiv\langle T_A\rangle$.

As an example, we consider the parameters associated with condensate observed in Ref. [8], where the mean frequency $\omega_o/2\pi\approx700$ Hz and $N=9\times10^5$. This yields $\hbar\omega$o

$=34.0$ nK, $d_A=0.79$ μm, $\eta_A=3.87\times10^3$, and $\Re=8.97$. The mean volume of the condensate is 1.47×10^{-9} cm^3, resulting in mean density of $\rho_A\approx6.1\times10^{14}$ cm^{-3}, which is in agreement with the measured initial density in Fig. 1 of Ref. [8]. The mean kinetic energy is equal to 2.07 nK, and equated to ϵ_0 predicts that $L\approx10.0$ μm.

As a check, we can use the observation in Ref. [7] that the condensate has an axial length of $L_{axis}=140$ μm and a waist formed by the dipole trap of $L_{waist}=6$ μm. Equating $4\pi L^3/3$ to the volume $(\pi L_{waist}^2 L_{axis}/4)\approx4.1\times10^{-9}$ cm^3, we estimate that $L\approx10$ μm, consistent with our determination from the kinetic-energy criterion.

[1] E. Tiesinga, B. J. Verhaar, and H. T. C. Stoof, Phys. Rev. A **47**, 4114 (1993).

[2] E. Tiesinga, A. J. Moerdijk, B. J. Verhaar, and H. T. C. Stoof, Phys. Rev. A **46**, R1167 (1992).

[3] A. J. Moerdijk, B. J. Verhaar, and A. Axelsson, Phys. Rev. A **51**, 4852 (1995).

[4] P. Courteille, R. S. Freeland, D. J. Heinzen, F. A. van Abeelen, and B. J. Verhaar, Phys. Rev. Lett. **81**, 69 (1998).

[5] F. A. van Abeelen, D. J. Heinzen, and B. J. Verhaar, Phys. Rev. A **57**, R4102 (1998).

[6] J. M. Vogels, C. C. Tsai, R. S. Freeland, S. J. J. M. F. Kokkelmans, B. J. Verhaar, and D. J. Heinzen, Phys. Rev. A **56**, R1067 (1997).

[7] S. M. Inouye, R. Andrews, J. Stenger, H.-J. Miesner, D. M. Stamper-Kurn, and W. Ketterle, Nature (London) **392**, 151 (1998).

[8] J. Stenger, S. Inouye, M. R. Andrews, H.-J. Miesner, D. M. Stamper-Kurn, and W. Ketterle, Phys. Rev. Lett. **82**, 2422 (1999).

[9] J. Weiner, V. S. Bagnato, S. Zilio, and P. S. Julienne, Rev. Mod. Phys. **71**, 1 (1999).

[10] G. K. Brennen, C. M. Caves, P. S. Jessen, and I. H. Deutsch, Phys. Rev. Lett. **82**, 1060 (1999).

[11] D. Jaksch, H.-J. Briegel, J. I. Cirac, C. W. Gardiner, and P. Zoller, Phys. Rev. Lett. **82**, 1975 (1999).

[12] E. Timmermans, P. Tommasini, M. Hussein, and A. Kerman, Phys. Rep. **315**, 199 (1999); see also E. Timmermans, P. Tommasini, R. Cote, M. Hussein, and A. Kerman, LANL preprint, cond-mat/9804015; P. Tommasini, E. Timmermans, M. Hussein, and A. Kerman, LANL preprint, cond-mat/9805323.

[13] V. A. Yurovsky, A. Ben-Reuven, P. S. Julienne, and C. J. Williams, Phys. Rev. A **60**, R765 (1999).

[14] F. A. van Abeelen and B. J. Verhaar, Phys. Rev. Lett. **83**, 1550 (1999).

[15] J. Javanainen and M. Mackie, Phys. Rev. A **59**, R3186 (1999).

[16] H. T. C. Stoof, J. M. V. A. Koelman, and B. J. Verhaar, Phys. Rev. B **38**, 4688 (1988).

[17] U. Fano, Phys. Rev. **124**, 1866 (1961).

[18] U. Fano and A. R. P. Rau, *Atomic Collisions and Spectra* (Academic Press, Orlando, FL, 1986).

[19] E. P. Wigner, Phys. Rev. **73**, 1002 (1948).

[20] P. S. Julienne and F. H. Mies, J. Opt. Soc. Am. B **6**, 2257 (1989).

[21] C. Cohen-Tannoudji, B. Diu, and F. Laloe, *Quantum Mechanics* (Wiley, New York, 1977), Vol. 1.

[22] A. L. Fetter and D. L. Feder, Phys. Rev. **58**, 3185 (1998).

[23] In practice we used $U_{trap}=c(R-L)$, with $c/k_B\approx0.75$ mK/a_o for $R>L$ which is steep enough to simulate an infinite wall, but soft enough not to cause numerical problems.

[24] D. R. Bates, *Quantum Theory I. Elements* (Academic Press, New York, 1961), p. 293.

[25] Y. Kayanuma and S. Fukuchi, J. Phys. B **18**, 4089 (1985).

[26] V. A. Yurovsky and A. Ben-Reuven, J. Phys. B **31**, 1 (1998).

[27] N. F. Mott and H. S. W. Massey, *The Theory of Atomic Collisions*, 3rd ed. (Oxford University Press, London, 1965).

[28] T. Laue, Ch. Saműlis, H. Knőckel, and E. Tiemann (private communication).

[29] E. Tiesinga, C. J. Williams, P. S. Julienne, K. M. Jones, P. D. Lett, and W. D. Phillips, J. Res. Natl. Inst. Stand. Technol. **101**, 505 (1996).

[30] F. A. van Abeelen and B. J. Verhaar, Phys. Rev. A **59**, 578 (1999).

[31] A. Crubellier, O. Dulieu, F. Masnou-Seeuws, M. Elbs, H. Knockel, and E. Tiemann, Eur. Phys. J. D **6**, 211 (1999).

[32] Magnetic field B is given in the SI unit mT (millitesla), and 10 G = 1 mT.

[33] F. H. Mies, J. Chem. Phys. **80**, 2514 (1984).

[34] F. H. Mies and P. S. Julienne, J. Chem. Phys. **80**, 2526 (1984).

[35] From a separate MQDT analysis of the resonances, we find $|s(B)\rangle\approx0.148|2\rangle+0.185|3\rangle+0.758|4\rangle+0.607|5\rangle|w(B)\rangle\approx0.014|2\rangle+0.017|3\rangle-0.630|4\rangle+0.777|5\rangle$.

[36] A. L. Fetter and D. L. Feder, Phys. Rev. A **58**, 3185 (1998).

[37] M. T. DePue, C. McCormick, S. L. Winoto, S. Oliver, and D. S. Weiss, Phys. Rev. Lett. **82**, 2262 (1999).

[38] R. Napolitano, J. Weiner, C. J. Williams, and P. S. Julienne, Phys. Rev. Lett. **73**, 1352 (1994).

[39] A. Vardi, D. Abrashkevich, E. Frishman, and M. Shapiro, J. Chem. Phys. **107**, 6166 (1997).

[40] P. S. Julienne, K. Burnett, Y. B. Band, and W. C. Stwalley, Phys. Rev. A **58**, R797 (1988).

[41] R. H. Wynar, R. S. Freeland, D. J. Han, and D. J. Heinzen (unpublished).

[42] D. J. Heinzen, R. H. Wynar, P. D. Drummond, and K. V. Kherunstyan (unpublished).

[43] B. I. Schneider and D. L. Feder, Phys. Rev. A **59**, 2232 (1999).